Review

Control of interface functions in solid-state biosensors for stable detection of molecular recognition

By Miyuki TABATA[*1] and Yuji MIYAHARA[*2,†]

(Edited by Shigekazu NAGATA, M.J.A.)

Abstract: Significant progress has been achieved in the field of solid-state biosensors over the past 50 years. Various sensing devices with high-density integration and flexible configuration, as well as new applications for clinical diagnosis and healthcare, have been developed using blood, serum, and other body fluids such as sweat, tears, and saliva. A high-density array of ion-sensitive field effect transistors was developed by exploiting the advantages of advanced semiconductor technologies and commercialized in combination with an enzymatic primer extension reaction as a DNA sequencer in 2011. Different types of materials such as inorganic materials, metals, polymers, and biomolecules are mixed together on the surface of the gate while maintaining their own functions; therefore, compatibility among different materials has to be optimized so that the best detection performance of solid-state biosensors, including stability and reliability, is achieved as designed. Solid-state biosensors are suitable for the rapid, cost-effective, and noninvasive identification of biomarkers at various timepoints over the course of a disease.

Keywords: ISFET, molecular recognition, biosensor, semiconductor device, surface modification, liquid biopsy

1. Introduction

Outstanding, rapid advances have been made in the field of microelectronics during the past 70 years. Highly reliable and functional chips can now be easily fabricated using a precisely controlled production process. Inexpensive microcomputers with high performance are now available, providing us with access to an abundance of various kinds of information.

While a metal-oxide-semiconductor field effect transistor (MOSFET) is one of the most fundamental devices in large-scale integrated circuits, a field effect transistor (FET) without a metal gate electrode was reported to be used in a physiological aqueous solution and the drain current was found to be sensitive to the sodium ion concentration in 1970.[1)] This device was named an ion-sensitive field effect transistor (ISFET).

[*1] Graduate School of Bio-Applications and Systems Engineering, Tokyo University of Agriculture and Technology, Koganei, Tokyo, Japan.

[*2] Institute of Biomaterials and Bioengineering, Tokyo Medical and Dental University, Tokyo, Japan.

† Correspondence should be addressed to: Y. Miyahara, Institute of Biomaterials and Bioengineering, Tokyo Medical and Dental University, 2-3-10 Kanda-surugadai, Chiyoda-ku, Tokyo 101-0062, Japan (e-mail: miyahara.bsr@tmd.ac.jp).

Non-standard abbreviation list: 10-CDT: 10-carboxy-1-decanethiol; APTES: 3-aminopropyltriethoxysilane; ATP: adenosine triphosphate; BSA: bovine serum albumin; CMOS: complementary metal oxide semiconductor; CRP: C-reactive protein; CTC: circulating tumor cells; CWE: coated wire electrode; DAPI: 4′,6-diamidino-2-phenylindole; dNTP: deoxynucleotide triphosphate; DOS: bis-(2-ethylhexyl)sebacate; ECM: extracellular matrix; EGFET: extended-gate field effect transistor; EGFR: epidermal growth factor receptor; ELISA: enzyme-linked immunosorbent assay; EMF: electromotive force; EMT: epithelial–mesenchymal transition; EpCAM: epithelial cell adhesion molecule; ETH2112: 3,3,4,4-benzhydroltetracarboxylate; EV: extracellular vesicle; FACS: fluorescence-activated cell sorting; FET: field effect transistor; GOD: glucose oxidase; GTP: guanosine triphosphate; ISE: ion-selective electrode; ISFET: ion-sensitive field effect transistor; miRNA: microRNA; MOSFET: metal-oxide-semiconductor field effect transistor; NaCl: sodium chloride; OH-PVC: vinyl chloride-vinyl alcohol copolymer; PCR: polymerase chain reaction; PDTA·Fe(III): 1,3-diaminopropanetetraacetic acid ferric ammonium salt monohydrate; PVA: polyvinyl alcohol; PVC: polyvinyl chloride; SAM: self-assembled monolayer; SB: sulfobetaine; SNP: single-nucleotide polymorphism; SOS: silicon-on-sapphire; THF: tetrahydrofuran; TOTM: tri-(2-ethylhexyl)trimellitate; XPS: X-ray photoelectron spectroscopy.

doi: 10.2183/pjab.100.004

Mechanical devices with three-dimensional structures were fabricated using the silicon etching technique to realize a miniaturized gas chromatograph system,[2] a glucose sensor,[3] and a liquid chromatograph system.[4] After these early studies, various types of solid-state biosensors have been developed using semiconductor technologies in combination with specific molecular recognition using enzymes, antibodies, nucleic acids, and cells.

Since the Human Genome Project started in 1990, new methods and devices for processing a large amount of biological information, such as DNA chips, microarrays, and bioinformatics, have been developed. Photolithography has been used to fabricate high-density DNA chips for gene expression analysis.[5] In 2011, massive parallel DNA sequencing was developed and commercialized based on a high-density transistor-array chip for a cost-effective, faster, and simpler genome analysis system.[6] The reductions in cost and time required for DNA sequencing have had a major impact on clinical research and medicine for realizing personalized therapeutic strategies.

The major advantages of using semiconductor technology to fabricate sensing devices are miniaturization of the device and integration of multiple sensing elements and signal processing circuits in a single chip. It is therefore possible to obtain information from a single cell and to access a single molecule by designing an appropriate structure and geometry of the sensing devices. It is also possible to detect multiple analytes in a parallel way using a high-density array of sensing devices.

Various types of solid-state biosensors using ISFETs have been reported in combination with biomolecular recognition reactions.[7,8] In these biosensors, biomolecular recognition reactions have been designed and performed on carriers such as membranes, beads, or cells on the gate of the ISFET. Because different types of materials such as inorganic materials, metals, polymers, and biomolecules are formed and integrated on the surface of the gate, compatibility among different materials has to be taken into consideration from the perspectives of rational mechanism and the principle of operation as potentiometric biosensors. The development of diverse solid-state biosensors has been achieved over the past few decades, and several review papers have been published in the fields of ion sensors,[9] electrochemical sensors,[10,11] biosensors,[12,13] and wearable sensors.[14,15] In this review, we focus on the progress of solid-state potentiometric biosensors and mainly discuss the design of the materials and chemical modification on the gate surface of ISFETs for achieving stable signal transduction.

2. Design of the interface between solid-state materials and ion-selective polymeric membranes

2.1. Solid-state ion sensor. Metal oxides or silicon nitride is usually formed on the surface of the gate area of an ISFET as a proton-selective membrane, while metals are usually used for a coated wire electrode (CWE) and an extended-gate FET (EGFET). To fabricate solid-state ion sensors for the detection of a variety of ions, ion-selective polymeric membranes are usually formed on the surface of metal oxides of ISFETs or the metals of CWEs and EGFETs, while an internal electrolyte solution is placed in contact with an ion-selective membrane for the conventional ion-selective electrode (ISE), as illustrated in Fig. 1. The signal line of an ISE is connected to a gate of a MOSFET of an input circuit in an operational amplifier. In the case of a CWE, an ion-selective membrane is directly formed on the surface of a metal electrode (a wire or

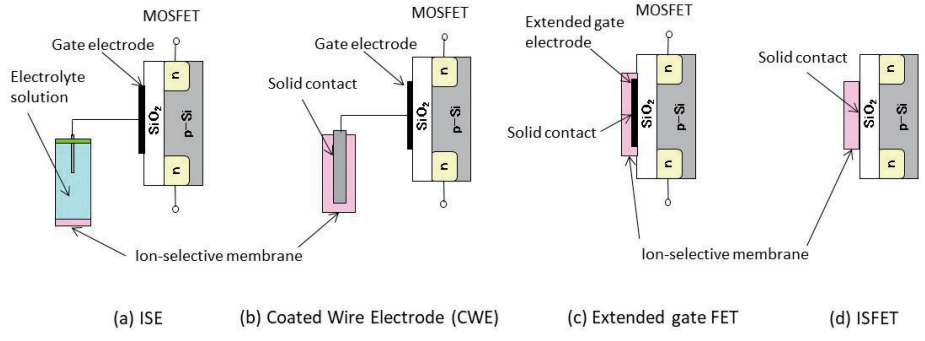

Fig. 1. Device configuration of ion sensors using an ion-selective polymeric membrane. (a) ISE. (b) Coated wire electrode (CWE). (c) Extended-gate FET. (d) ISFET.

a substrate) without an internal electrolyte solution. The signal line of a CWE is connected to a gate of a MOSFET. A metal electrode and a signal line are fabricated on the same chip as a MOSFET in the case of EGFET and an ion-selective membrane is formed at the end of the extended-gate metal electrode. In the case of ISFET reported earlier, an ion-selective polymeric membrane is directly formed on the surface of a pH-sensitive material such as Si_3N_4, Al_2O_3, or Ta_2O_5 without any metal electrode. The major difference between a conventional ISE and solid-state ion sensors is that one of the surfaces of the ion-selective membrane is in direct contact with solid materials in solid-state ion sensors, while both surfaces of the ion-selective membrane are in contact with an aqueous electrolyte solution in an ISE.

A solid-state ion sensor with an ion-selective polymeric membrane was first reported in the form of CWE in 1971,[16] and an ISFET with an ion-selective polymeric membrane directly coated on the gate insulator was reported in 1975.[17] Since then, various types of solid-state ion sensors with different ion-selective membranes have been reported. Although the fundamental characteristics of the early solid-state ion sensors, such as slope sensitivity and selectivity, were similar to those of conventional ISEs, commonly observed phenomena in the solid-state ion sensors were a shift and drift of the electromotive force (EMF).[18)–23)] Several mechanisms such as leaching of ionophores from the ion-selective membrane, water uptake in the ion-selective membrane, and a redox reaction at the internal metal electrode were considered to explain the EMF behaviors of solid-state ion sensors.[24),25)] In the case of ISFETs, formation of a thin water layer at the interface between an ion-selective polymeric membrane and the gate insulator of an ISFET was experimentally confirmed.[26)] Carbon dioxide in the air was considered to penetrate the ion-selective polymeric membrane and change the pH in the thin water layer at the interface. This would considerably affect the response behavior of the ISFET. Meanwhile, one of the reasons suggested was the lack of thermodynamic equilibrium between the ion-selective membrane and the solid material.[27)] To make a system similar to a conventional ISE, hydrophilic intermediate layers such as hydrated polyvinyl alcohol,[27)] dextran,[21)] and poly(hydroxylethyl metacrylate)[28)] were proposed to be introduced between the ion-selective membrane and a solid material, because all interfaces were thermodynamically defined in the ISE.[29)] In many cases, the interface between an ion-selective membrane and a solid material was a point of discussion and would play an important role in understanding the EMF behavior of solid-state ion sensors.

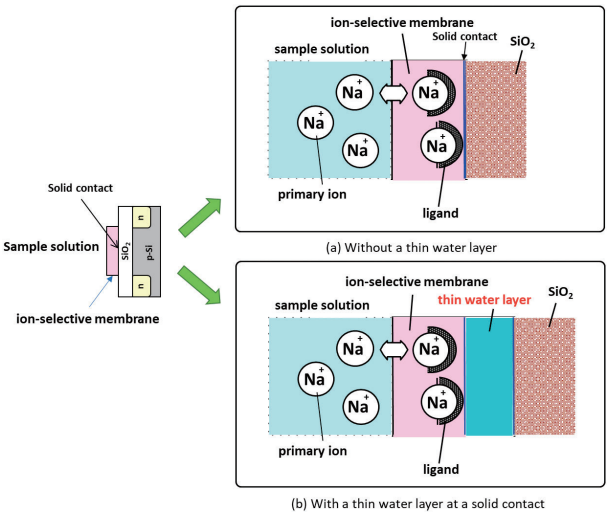

Fig. 2. Schematic of the cross section of a solid-state ion sensor with or without a water layer. (a) Without a thin water layer. (b) With a thin water layer at a solid contact.

2.2. EMF behaviors of solid-state ion sensors. Figure 2 shows a schematic cross section of a solid-state ion sensor with and without a thin water layer. A thin water layer is formed at the interface between the ion-selective polymeric membrane and a solid material, and is regarded as an additional internal layer.[30)] Therefore, two additional interfaces are generated in the system, that is, the interface between the ion-selective polymeric membrane and the thin water layer, and the one between the thin water layer and the solid material. Both interfaces of the thin water layer should be investigated in order to understand the EMF behavior and instability mechanism of solid-state ion sensors. First, the EMF behaviors of ISFETs with a potassium-ion-selective membrane were compared with those of ISEs with an internal electrolyte solution.[22)] Materials and compositions of the ion-selective membranes used in the experiments are listed in Table 1. Membrane components, including matrix, plasticizer, and ligand, were homogeneously mixed in a tetrahydrofuran (THF) solution. We used valinomycin as a ligand, polyvinyl chloride (PVC) or vinyl chloride-vinyl alcohol copolymer (OH-PVC) as a matrix, and bis-(2-ethylhexyl)sebacate (DOS), tri-(2-ethylhexyl)trimellitate (TOTM), or 3,3,4,4-benzhydroltetracarboxylate (ETH2112) as a plasticizer. Fabrication methods

Table 1. Materials and composition of ion-selective membranes. Reprinted from Electroanalysis, **3**, (1991) 287–292 with permission from John Wiley and Sons

Function	Materials	Composition [wt%]
Matrix	PVC OH-PVC	33
Plasticizer	DOS TOTM ETH2112	66
Ligand	Valinomycin	1

of the ion-selective membranes for ISEs and ISFETs were described elsewhere in detail.[22)]

The slopes, selectivity factors, drifts, and hysteresis of ISFETs and ISEs with different types of ion-selective membranes are summarized in Table 2. The slope of the ISFET with PVC/DOS or PVC/TOTM membrane was 57.27 or 56.49 mV/decade, respectively, which was good in terms of the theoretical slope (59.2 mV/decade at 25 °C). If slopes and selectivity factors of ISFETs were compared with those of corresponding ISEs, slopes of ISFETs were smaller than those of corresponding ISEs and selectivities were not as good as those of corresponding ISEs. Unless membranes for both ISFETs and ISEs were prepared from the same cocktails and compared at the same time, identifying the differences in slope and selectivity between ISFETs and ISEs was difficult because the observed differences were small. Meanwhile, differences of drifts and hysteresis were significant. The values of drifts and hysteresis of ISFETs as well as deviations from the average values were larger than those of ISEs.[22)]

Fundamental characteristics of solid-state ion sensors were further investigated using the form of CWE. A silver-silver chloride electrode was used as a solid-state electrode. The interface between an ion-selective polymeric membrane and a silver-silver chloride electrode was modified by introducing polyvinyl alcohol (PVA) layers, each with a different concentration and a different kind of electrolyte salt, into the interface.[31)] The hydrophilic PVA layer was in a dry state before the outer surface of the ion-selective membrane came into contact with an aqueous solution. The effects of this modification of the interface on the shift and drift of EMFs of solid-state ion sensors were investigated to elucidate potential-determining processes at the interface. In this experiment, solid-state ion sensors based on a sodium-ion-selective membrane were evaluated. The sodium-ion-selective membrane consisted of bis[(12-crown-4)methyl]-2-dodecyl-2-methylmalonate as a ligand, polyvinyl chloride as a matrix, dioctyl adipate as a plasticizer, and sodium tetraphenylborate as an

Table 2. Comparison of fundamental characteristics between ISFET and ISE. Reprinted from Electroanalysis, **3**, (1991) 287–292 with permission from John Wiley and Sons

(a) Characteristics of K^+-ISFETs with different membranes containing valinomycin

Sample	Slope	Selectivity Factor, $\log K^{pot}$						Drift	Hysteresis
	(mV/decade)	H^+	Li^+	Na^+	NH_4^+	Mg^{2+}	Ca^{2+}	(mV/h)	(mV)
PVC/DOS	57.27	−3.38	−3.68	−3.48	−1.94	−3.73	−4.21	−0.237	14.67
PVC/TOTM	56.49	−3.54	−3.35	−3.38	−1.85	−3.69	−3.95	0.189	−5.81
PVC/2112	47.6	−2.8	−3.14	−2.9	−1.55	−3.48	−3.2	0.154	−2.73
OH-PVC/DOS	52.26	−3.95	−3.79	−2.62	−1.71	−3.96	−4.17	−0.955	4.38
OH-PVC/TOTM	52.88	−3.6	−3.02	−3.22	−1.74	−3.41	−3.93	−0.193	1.89
OH-PVC/2112	46.91	−3.72	−3.46	−2.47	−1.67	−3.05	−3.88	2.3	1.8

(b) Characteristics of K^+-ISEs with different membranes containing valinomycin

Sample	Slope	Selectivity Factor, $\log K^{pot}$						Drift	Hysteresis
	(mV/decade)	H^+	Li^+	Na^+	NH_4^+	Mg^{2+}	Ca^{2+}	(mV/h)	(mV)
PVC/DOS	58.42	−4.65	−4.47	−3.92	−1.87	−4.97	−4.5	−0.011	−0.32
PVC/TOTM	57.89	−4.75	−4.8	−4.09	−2.04	−4.92	−4.82	0.012	0.41
PVC/2112	51.67	−3.42	−3.61	−3.33	−1.48	−4.1	−3.89	0.018	−0.12
OH-PVC/DOS	55.5	−3.69	−3.53	−2.4	−1.82	−3.44	−3.98	0.013	−0.97
OH-PVC/TOTM	54.76	−3.71	−3.54	−2.25	−1.83	−3.47	−3.99	0.02	0.34
OH-PVC/2112	49.01	−3.33	−3.23	−2.4	−1.55	−3.24	−3.65	0.024	−0.55

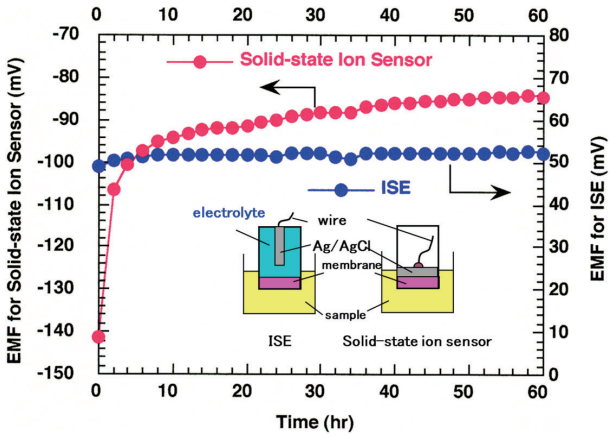

Fig. 3. Typical drift characteristics of ion sensors. Reprinted from Anal. Chim. Acta, **331**, (1996) 85–95 with permission from Elsevier.

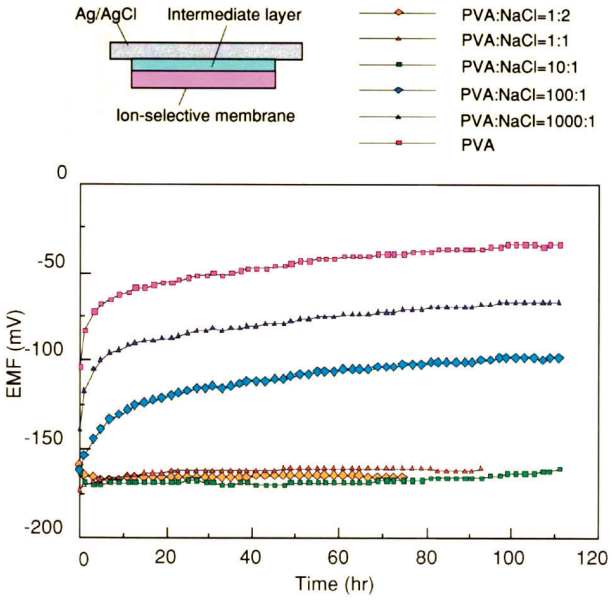

Fig. 4. EMF behaviors of the solid-state sodium ion sensors with different concentrations of sodium chloride in the intermediate layer. Reprinted from Anal. Chim. Acta, **331**, (1996) 85–95 with permission from Elsevier.

additive. To investigate the role of the interface between an ion-selective membrane and a silver-silver chloride electrode, sodium chloride, potassium chloride, potassium bicarbonate, and potassium acetate were used as electrolyte salts in a thin PVA layer. The thickness of the PVA layer was approximately 55 μm.

EMF behaviors of both a solid-state ion sensor without an intermediate layer and an ISE are shown in Fig. 3.[31] A 0.1 M NaCl solution was used as the internal solution for the ISE, in which a silver-silver chloride electrode was placed. The EMF of the solid-state ion sensor was more negative (by 140 mV) than that of the ISE. These EMF behaviors can be characterized using the initial EMF change within 10 hours and the steady-state drift after 15 hours. The initial EMF change of the solid-state ion sensor was 46 mV, whereas that of the ISE with an internal solution was 3 mV. The steady-state drift of the solid-state ion sensor was 0.2 mV/h, whereas that of the ISE was 0.03 mV/h. These are typical examples of the shifts and drifts of EMFs for a conventional solid-state ion sensor without an intermediate layer and the ISE.

2.3. Role of the interface between a solid and an ion-selective membrane. To investigate the roles of ions at the interface between the ion-selective membrane and the silver-silver chloride electrode for the EMF of a solid-state sodium ion sensor, a dried hydrophilic intermediate layer of PVA containing different amounts of sodium chloride (NaCl) was interposed between them. Time courses of the EMFs of solid-state sodium ion sensors are shown in Fig. 4.[31] The weight ratio between NaCl and PVA, NaCl/PVA, in the intermediate layer was changed from 1/1000 to 2. When an aqueous solution was introduced onto the surface of ion-selective membranes of the sensor, water molecules diffuse through the ion-selective membrane to the intermediate layer.[31] The intermediate layer absorbs water molecules and any NaCl in the layer is dissolved and ionized. As a result, the intermediate layer serves as an internal electrolyte solution; that is, sodium ions in the layer can exchange with the ion-selective membrane and chloride ions can exchange with the silver-silver chloride electrode. As a result of efficient exchange of charged ions at the phase boundaries, the solid-state ion sensors are considered to reach an equilibrium, showing a stable EMF. As shown in Fig. 4, the EMFs of solid-state ion sensors were significantly dependent on the weight ratio. When the content of NaCl in the intermediate layer was sufficiently high (weight ratios were 1/10, 1, and 2), the EMFs of solid-state ion sensors were almost constant at −170 mV. This EMF value corresponded to that of ISE with a saturated internal electrolyte solution. Therefore, ion concentrations in the intermediate layer were estimated to be saturated when a sufficient amount of salts was incorporated into the layer. Meanwhile, when the weight ratio was 1/100 and 1/1000, the EMF increased as the amount of NaCl in the intermediate layer decreased. In this

case, the ion concentrations in the intermediate layer were considered not to be saturated and the EMFs were dependent on the concentration of NaCl in the intermediate layer.

Drift characteristics of solid-state ion sensors were also significantly dependent on the weight ratio between NaCl and PVA in the intermediate layer.[32] When the concentration of NaCl was saturated in the intermediate layer, the EMF of solid-state ion sensors was stable and almost constant over the evaluation period. The initial EMF changes and steady state drifts were smaller than 10 mV and about 0.05 mV/h, respectively. Meanwhile, when the weight ratio was 1/100 or 1/1000, the EMF of solid-state ion sensors showed significant drift. The initial EMF changes and steady-state drift of these sensors were greater than 50 mV and 0.2 mV/h, respectively. It was assumed that the reason for the large drift for sensors with small weight ratios was that the ion concentration in the intermediate layer changed with time depending on the amount of water absorbed.

The solid-state sodium ion sensor showed a large drift even if a hydrophilic intermediate layer was placed between the ion-selective liquid membrane and the silver-silver chloride electrode. The initial EMF change and the drift of the solid-state sodium ion sensor were small only when the hydrophilic intermediate layer contained a sufficient amount of NaCl. This indicated that the primary ions, sodium ions in this case, need to be exchanged between the ion-selective membrane and the intermediate layer, and that chloride ions need to be exchanged between the intermediate layer and the silver-silver chloride electrode for the stable EMF of the solid-state ion sensor. In the case of conventional solid-state ion sensors in which an ion-selective liquid membrane is in direct contact with a solid-state electrode, charged species cannot be exchanged efficiently between the ion-selective membrane and thin water layer, or between the thin water layer and solid-state electrode. It was found that this was the main reason for the shift and drift of EMF of solid-state ion sensors. To stabilize the EMF of solid-state ion sensors, efficient ion exchange and electrochemical equilibrium should be established at all of the phase boundaries of an ion-selective liquid membrane and solid electrode, as illustrated in Fig. 5.[21),31)] A variety of materials and mechanisms for solid contacts have been proposed for the phase boundaries to realize stable solid-state ion sensors.[9),33)]

Recently, wearable sensors have been attracting considerable attention for continuous real-time health monitoring.[34)] Various solid-state ion sensors have been developed for real-time and noninvasive monitoring of electrolytes and metabolites in sweat, tears, or saliva as indicators of health status. Typical examples of the analytes are glucose, lactate, Na^+, K^+, H^+, NH_4^+, Ca^{2+}, and Cl^-, many of which correlate with their concentrations in blood.[35)] From the perspective of practical operation, a calibration process is required using standard solutions containing known concentrations of analytes for most solid-state biosensors to precisely determine the analyte concentration. In the case of wearable sensors, calibration cannot be performed frequently during the measurements, although one-point calibration (baseline correction) is usually carried out for blood/serum electrolyte measurements for every sample in clinical testing. Stability of the output signals of solid-state biosensors is required for long-term measurement, while calibration-free sensors have been reported in the field of ISEs.[36),37)] Solid-contact ISEs are an active research area in the field of ISEs because they are readily applicable to wearable sensors.

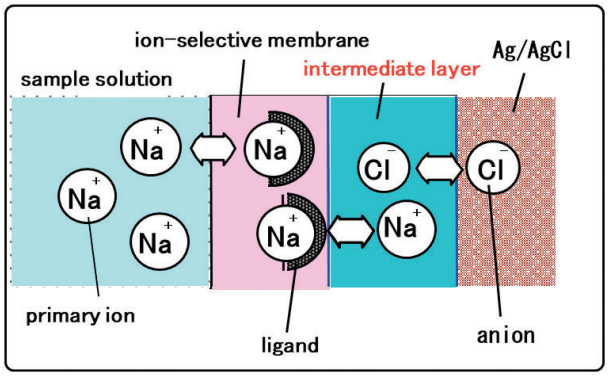

Fig. 5. Schematic of the cross section of a solid-state ion sensor with an intermediate layer containing a sufficient amount of sodium chloride.

3. Inorganic and organic mixed phase materials for immobilization and detection of biomolecules

3.1. Design of a self-assembled monolayer/AgCl electrode. Taking advantage of large-scale integration of solid-state biosensors, a high-density array of extended-gate ISFETs has been used in a DNA sequencer.[6)] Gold is often used as a material for the extended-gate electrode. Not only is the extended-gate ISFET compatible with complementary metal oxide semiconductor (CMOS) technology, but gold also has excellent affinity for SH groups, making it easy to immobilize biomolecules. Therefore, gold is

also used as the sensing surface for surface plasmon resonance[38),39)] and quartz crystal microbalance.[36),37)] Because the gold electrode becomes a polarized surface in aqueous solution, the EMF of the electrode changes due to the adsorption of charged chemical species such as ions.[40)] For this reason, gold is not necessarily suitable as an electrode material for potentiometric measurement, and there are problems of stability such as drift, shift, or variation of the EMF. When the surfaces of gate materials such as Si_3N_4 and Ta_2O_5 are in contact with aqueous solution, silanol groups and hydrates are formed at the surface of the gate materials, and the EMF at the solid-liquid interface is stabilized due to the electrochemical equilibrium of these dissociative groups. Although organosilicon derivatives such as alkyl aminosilanes are often used to functionalize the metal oxide surface,[41)–43)] high-quality self-assembled monolayers (SAMs) of organosilicon derivatives are not simple to produce, partly because of the need to carefully control reaction conditions such as the amount of water in solution[44)–46)] and multilayer formation.[47),48)] Therefore, controlling the density and orientation of immobilized biomolecules in a reproducible manner is difficult.[49)]

A new approach based on organic and inorganic mixed phase modification of the surface of silver has been proposed to realize an electrochemically defined interface capable of immobilizing biomolecules with controlled density and orientation.[40)] A SAM of an alkanethiol can be formed easily on the surface of silver for functionalization with biomolecules. At the same time, the EMF of the silver surface is easily stabilized by forming silver chloride. The structure and chemistry of alkanethiol SAMs on Ag(111) have previously been investigated in detail.[41),50)] The EMF of the silver/silver chloride electrode is stable and constant in the presence of fixed chloride ion concentrations. In many cases, the chloride ion concentration before and after the biomolecular recognition reaction can be considered constant in controlled *in vitro* measurement conditions. The SAM/silver and silver/silver chloride structures were mixed and integrated at the surface of a thin silver film to simultaneously achieve functionalization of biomolecules and stabilization of the EMF of the electrochemical biosensor. This organic and inorganic mixed surface of the thin silver film was applied to hybridization asseys, potentiometric detection of nucleic acids, for cancer diagnosis in liquid biopsies.[40)]

3.2. Characterization of SAM/AgCl mixed surface. Figure 6 shows a schematic of the cross section of an organic/inorganic mixed nanostructure formed on the silver surface. Alkanethiol groups are in direct contact with the silver surface, and the remaining silver surface is covered with silver chloride. The alkyl chains of the SAM of alkane thiolates on a clean Ag(111) surface are orientated practically perpendicular to the surface, whereas those prepared on an Au(111) surface are tilted at 26–28° from the surface normal.[41)] Sulfobetaine (SB) 3-undecanethiol or 10-carboxy-1-decanethiol (10-CDT) was first used to form a SAM on the surface of a sputtered thin silver film, followed by treatment with 1,3-diaminopropanetetraacetic acid ferric ammonium salt monohydrate [PDTA·Fe(III)] as an oxidizing agent to form a thin AgCl layer by chemically oxidizing the Ag surface. Functional groups of the alkanethiol can be used for the immobilization of biomolecules. The mixed SAM was prepared on the surface of the silver film using oligonucleotide- and SB-terminated alkanethiols, to control the DNA probe density and to maximize the efficiency and kinetics of hybridization.

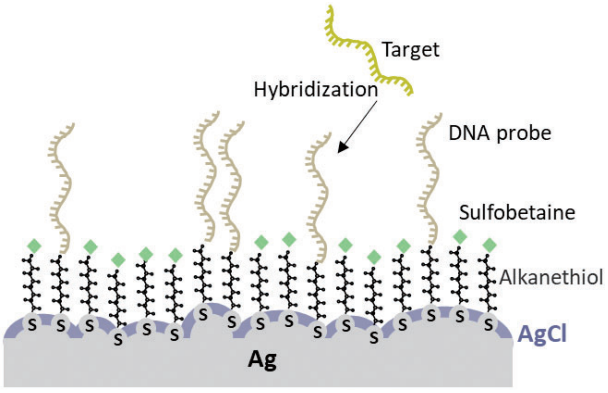

Fig. 6. Schematic of the cross section of the organic and inorganic mixed nanostructure. Reproduced from RSC Adv., **11**, (2021) 24958–24967 with permission from the Royal Society of Chemistry.

X-ray photoelectron spectroscopy (XPS) measurements were performed for detailed elemental analysis of organic and inorganic nanostructure surfaces. Figure 7 shows changes in the XPS spectra of Cl 2p derived from AgCl, and S 2p and C 1s derived from thiol groups when the SAM concentration was changed to 1 µM, 5 µM, and 10 µM. The peak intensity in the Cl 2p spectra decreased with increasing 10-CDT solution concentration, which indicated increasing surface coverage of the SAM for a higher concentration of 10-CDT. The peak intensities in the S 2p and C 1s spectra increased

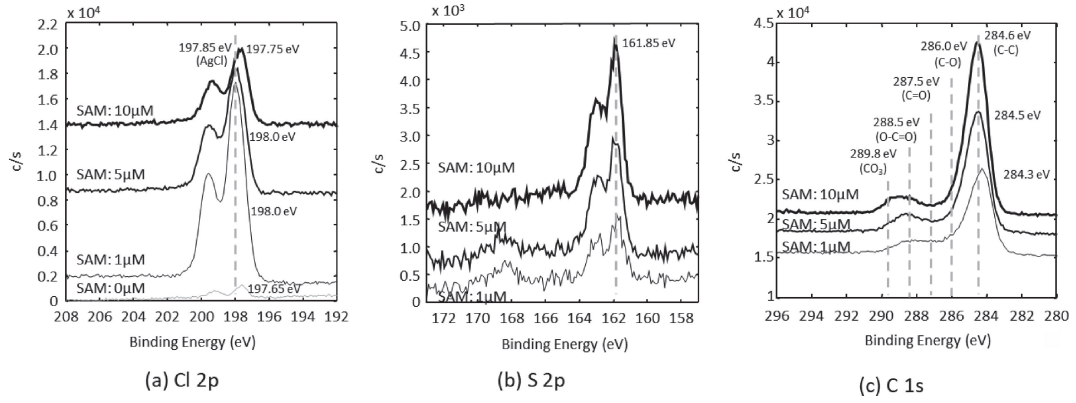

Fig. 7. XPS spectra of organic and inorganic mixed nanostructure surfaces containing SAMs and silver chloride. (a) Cl 2p. (b) S 2p. (c) C 1s. Reproduced from RSC Adv., **11**, (2021) 24958–24967 with permission from the Royal Society of Chemistry.

with increasing 10-CDT concentration because of the increasing SAM density. By changing the concentration of the SAM solution, the mixing ratio of the SAM and silver chloride phases formed on the silver surface can be controlled. Control and optimization of DNA probe density are important for nucleic acid detection by DNA hybridization. There is a trade-off between high sensitivity due to high density of DNA probes and inhibition of hybridization due to steric hindrance between adjacent probes. In the SAM/silver chloride mixed nanostructure, the density of DNA probes is controlled by forming mixed SAMs by changing the SAM concentration and the mixing ratio between sulfobetaine3-undecanethiol and oligonucleotide-terminated alkanethiols.

Zwitterionic SB has antifouling characteristics and can dramatically reduce the nonspecific adsorption of proteins.[51),52)] To confirm the orientation of the functional group of the SAM, the antifouling effect of the organic/inorganic mixed nanostructure was evaluated for protein adsorption using a 10-CDT SAM or a sulfobetaine3-undecanethiol SAM. Figure 8 shows the nonspecific adsorption of bovine serum albumin (BSA) on the above surfaces after direct contact with 10 μg/ml, 100 μg/ml, and 1 mg/ml BSA solutions. The amount of BSA adsorbed on the SB-SAM surface was low even after the chemical deposition of silver chloride with 2 mM PDTA treatment, whereas a large amount of BSA was adsorbed on the silver and 10-CDT-SAM surfaces. This indicated that the orientation of SB-SAM was maintained with the SB group exposed on the surface. Less BSA adsorption on the SB-terminated SAM was thus confirmed, even after the chemical deposition of silver chloride.[40)]

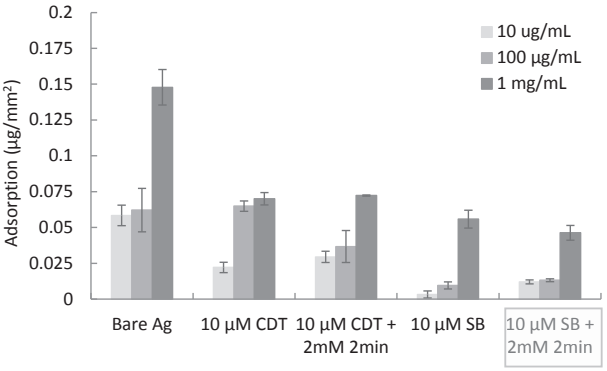

Fig. 8. Evaluation of nonspecific adsorption of BSA on different modified surfaces. Reproduced from RSC Adv., **11**, (2021) 24958–24967 with permission from the Royal Society of Chemistry.

3.3. Potentiometric hybridization assay. The EMF of the organic/inorganic mixed nanostructure with oligonucleotide probes was monitored during hybridization in real time. The difference in EMF between before and after hybridization, based on the negative charge of the nucleic acid, was used as a potential signal of hybridization. In the hybridization experiments, the complementary DNA of microRNA 146a (miR-146a) was employed as a model detection target. Figure 9 shows changes in potential response when the concentration of target DNA was changed. The EMF signals for hybridization were about −15 mV for higher concentrations of target DNA. It should be noted that the standard deviations of the EMFs were sufficiently small, even after hybridization and washing with 100 mM NaCl solution. On the basis of these results, the limit of detection was determined to be 0.1 pM for the

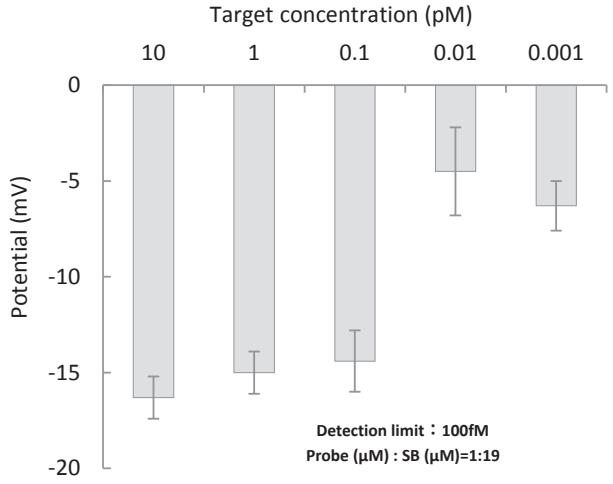

Fig. 9. Effect of target DNA concentration on EMF response of an organic and inorganic mixed nanostructure. Reproduced from RSC Adv., **11**, (2021) 24958–24967 with permission from the Royal Society of Chemistry.

organic and inorganic mixed phase structure, whereas that of the mixed SAM with oligonucleotide probes on the surface of a conventional thin gold film electrode was 20 pM.[53] The signal to noise ratio was 9.1 at a concentration of 0.1 pM, which was higher than that reported previously for potentiometric nucleic acid detection. These results demonstrated that stable and reliable detection of a microRNA with high sensitivity was achieved using an organic and inorganic mixed phase surface.

4. Signal transduction schemes for potentiometric detection irrespective of Debye screening

4.1. Debye screening effect. In the case of potentiometric detection of charged molecules based on the FET format, detecting the change in charge density induced outside the electric double layer is impossible because this change is shielded by counter ions. The width of the electric double layer, that is, the Debye length, is expressed using the following equation.

$$\delta = (\varepsilon\varepsilon_0 kT/2q^2I)^{1/2} \quad [1]$$

Here, δ represents Debye length; ε, relative permittivity; ε_0, vacuum permittivity; k, Boltzmann constant; T, absolute temperature; q, electric charge; and I, ionic strength. As can be seen from Eq. [1], the Debye length δ is a function of ionic strength. In a simple solution such as NaCl solution, δ is about 1 nm at a concentration of 100 mM and about 10 nm at a concentration of 1 mM. To ensure sensitivity, the ionic strength of the measurement solution and a molecular recognition reaction design that induces a large change in charge density within the Debye length needs to be optimized. Antibodies or antibody fragments are often used as capture molecules not only for biosensors but also in many biological analyses. Because the size of antibodies is generally on the order of several nanometers, they have not been frequently used as capture probes for potentiometric biosensors due to the Debye screening effect.[54]

4.2. Conformation change of aptamer. "Aptamer" is a general term for oligomeric sequences of nucleic acids and peptides that have selectivity and affinity comparable to those of antibodies for a specific molecule.[55] Because aptamers are not as large as antibodies, potentiometric biosensors using aptamers as new molecular recognition elements instead of antibodies are attracting attention. Nucleic acid aptamers can also be nanostructured by intramolecular base pairing and endowed with various functions such as responsiveness to stimuli. Taking advantage of these attributes of aptamers, a new detection scheme for potentiometric solid-state biosensors has been proposed using charged tag molecules, which goes beyond the limitations of Debye screening.

Specifically, the gate surface of an FET was modified with a hairpin DNA aptamer preloaded with a cationic DNA binder, and a detection scheme was designed so that the hairpin opened upon recognition of the target molecule, releasing the DNA binder into solution.[56] This detection scheme is not affected by the charge in the target molecule itself or the shielding effect of the Debye length of the solution. A schematic of biomolecule detection based on conformational changes in hairpin aptamers is shown in Fig. 10. An alkanethiol self-assembled film was formed on the surface of the gold electrode, which also served as the extended-gate electrode of the transistor, and 4′,6-diamidino-2-phenylindole (DAPI), a DNA binder, was captured in the double-stranded part of the hairpin structure of the nucleic acid aptamer in advance. In the experiment, an aptamer with high affinity to adenosine triphosphate (ATP) was used. When ATP to be detected was introduced into the sample solution, the aptamer captured ATP to shift to a more stable state, with accompanying conformational change, as illustrated in Fig. 10. At this time, DAPI bound to the double-stranded DNA was released. Because DAPI has a

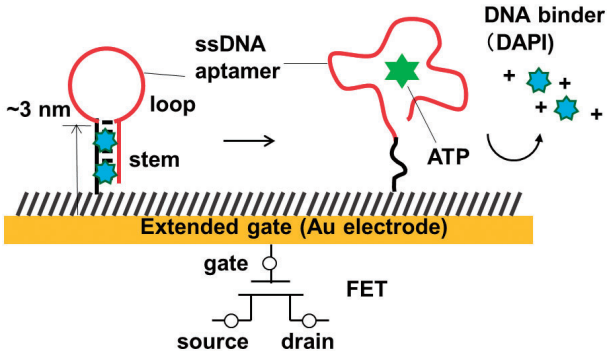

Fig. 10. Schematic of biomolecular detection based on conformational change in a hairpin aptamer. Reproduced from Biosens. Bioelectron., **32**, (2012) 244–249 with permission from Elsevier.

positive charge, its release changes the electrostatic state near the gate electrode interface. This electrical change is detected with an extended gold electrode in the proposed scheme. DAPI binds to the double-stranded portion of the hairpin aptamer near the gate electrode surface, and the molecular recognition reaction always induces an electrical change near the gate electrode surface within the electric double layer. Therefore, the problem of electrostatic shielding by counter ions associated with the Debye length is eliminated in this scheme. In addition, regardless of the charge of the biomolecule to be detected, the electrical change due to the release of positively charged DAPI is always induced upon molecular recognition; therefore, detecting electrically neutral biomolecules is possible.[56)]

Detection of ATP in comparison with guanosine triphosphate (GTP) based on three types of detection schemes is shown in Fig. 11. As shown in Fig. 11(a), the potential response to ATP changed in a concentration-dependent manner, but the response to GTP hardly changed. It was also confirmed that the response to ATP was not obtained with the hairpin aptamer alone or with the combination of the linear aptamer and DAPI, and that the combination of the hairpin aptamer and DAPI was essential to generate the concentration-dependent signals. Although ATP has negative charges due to phosphate ions, adenosine is an electrically neutral molecule and exhibits affinity to the same aptamer used in the experiments shown in Fig. 11. The responses of the proposed detection scheme to adenosine and guanosine are shown in Fig. 12. Guanosine is also an electrically neutral molecule. From Fig. 12, a concentration-dependent potential response may be obtained only to adenosine, confirming that the proposed scheme was also effective for electrically neutral molecules.[56)]

4.3. Stimulus-responsive polymer gel. A report has also been published of another approach to design molecular recognition using a stimulus-responsive polymer gel formed on the surface of a gate of an FET.[57)] This gel contained a dissociated phenylboronic acid group, which formed a reversible complex with a diol compound, and the apparent dissociation equilibrium of the phenylboronic acid group shifted due to changes in the surrounding glucose concentration. 4,3-Acrylamidophenylboronic acid, N-isopropylacrylamide, and a polymerization initiator were copolymerized to incorporate phenylboronic acid groups into a volume phase transition polymer gel network. Changes in glucose concentration induce ionic osmotic pressure in the polymer gel, which leads to a synchronized reversible volume phase transition.[58),59)] Most of the weight of hydrophilic acrylamide gels is due to water, and the change in the degree of swelling can be almost synonymous with the change in water content. The relative permittivity of water is approximately 80, whereas that of polymer chains in a condensed state is

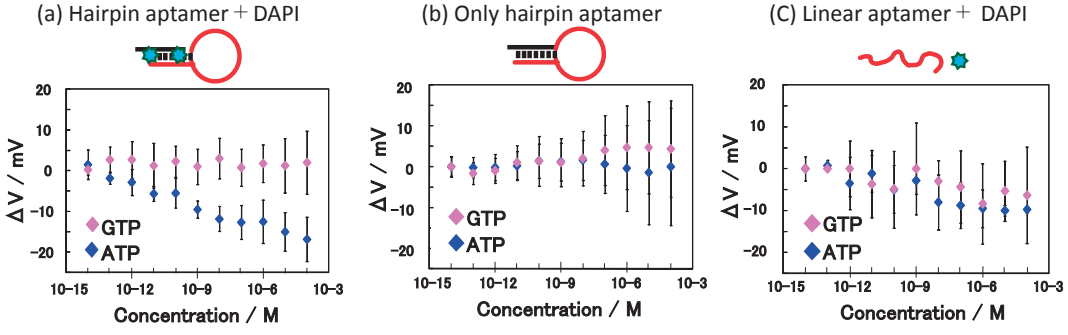

Fig. 11. Detection of ATP based of a conformational change of a hairpin aptamer. (a) Hairpin aptamer + DAPI. (b) Only hairpin aptamer. (c) Linear aptamer + DAPI. Reproduced from Biosens. Bioelectron., **32**, (2012) 244–249 with permission from Elsevier.

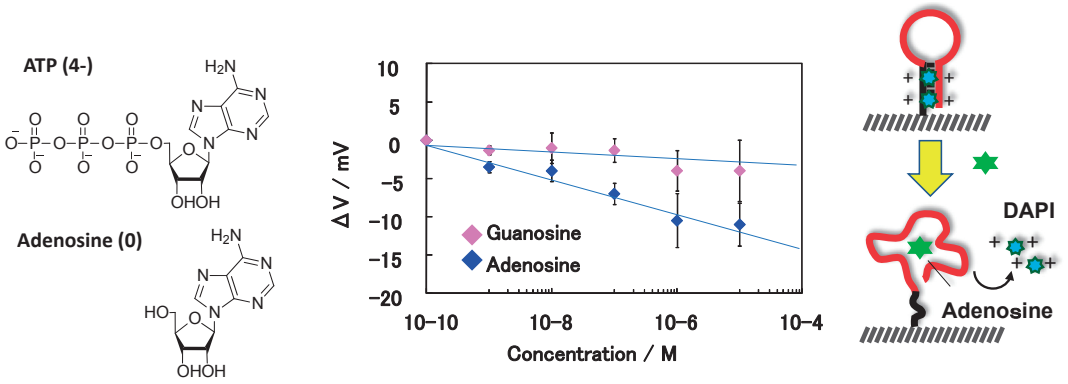

Fig. 12. Detection of electrically neutral adenosine using a conformational change of hairpin aptamer. Reproduced from Biosens. Bioelectron., **32**, (2012) 244–249 with permission from Elsevier.

approximately 2–3. Therefore, the change in apparent relative permittivity caused by water influx into the gel matrix is considered to play an important role in the signal transduction mechanism in the gel-modified gate FET. The output voltage of the transistor changed depending on the glucose concentration, and a reversible response was obtained.[57] Glucose is an electrically neutral biomolecule, which is difficult to detect by simple capture on the gate surface.

The change in threshold voltage, ΔV_T, which is one of the output forms of the transistor, is expressed by the change in charge density induced on the gate surface as a result of biomolecular recognition, ΔQ_{DL}, and the gate capacitance, C_I, as described in Eqs. [2] and [3].

$$\Delta V_T \propto (\Delta Q_{DL})/C_I \quad [2]$$

$$C_I = \varepsilon_0 \varepsilon A/d \quad [3]$$

Here, ε_0, ε, A, and d are vacuum permittivity, relative permittivity, gate area, and thickness of gate insulator, respectively. The biomolecule concentration can be calculated from the threshold voltage change and the charge density change of the biomolecule by assuming that the gate capacitance does not change before and after molecular recognition. Meanwhile, in an FET using a stimulus-responsive polymer gel, the threshold voltage change depends on the gate capacitance C_I, and the gate capacitance is related to the permittivity of the gate materials. As described above, the polymer gel introduced as one of the gate materials reacts with the molecule to be detected and causes a volume phase transition, which induces a change in permittivity (due to a change in the water content) of the gel. This detection scheme is another example of a transistor capable of Debye-length-independent detection of molecular recognition. The results demonstrated that not only charged molecules but also uncharged molecules such as glucose can be detected by adding the permittivity change as a detection parameter. On the basis of this principle, the detection of molecules other than glucose has been reported.[60),61)]

5. Detection of biomolecular recognition using ISFETs in combination with enzymatic signal amplification

When enzymes are used as the biologically active substance, changes in ion concentration produced by the enzyme-substrate reaction are measured with the ISFET.[62)] A differential detection scheme using an enzyme and a reference FETs is shown in Fig. 13. In most cases, proton-sensitive ISFETs have been used in combination with enzyme-substrate reactions that involve the consumption or production of hydrogen ions. Two examples of enzyme-substrate reactions for the detection of urea and glucose are described in Fig. 13. In both cases, local pH changes are induced by the enzymatic reactions. In these biosensors, enzymatic reactions have been designed and performed on carriers such as membranes, beads, or proteins on the gate of the ISFET. In this case, the points of hydrogen ion generation and consumption are not always in direct contact with the surface of the ISFET. Only some of the generated hydrogen ions diffuse to the surface of the gate and contribute to the signal generation of the ISFET. To efficiently and rapidly detect the pH change at the surface of the hydrogen ion-selective membrane, the design and materials of the immobilized enzyme carriers should be optimized. When the pH in the bulk of the sample

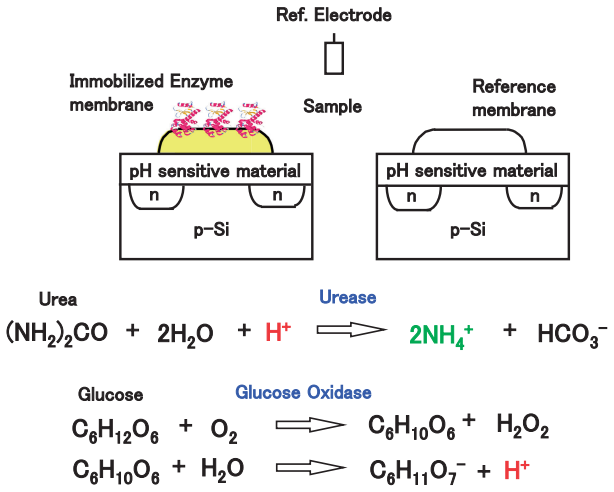

Fig. 13. Differential detection scheme using an enzyme and a reference FETs. An immobilized enzyme membrane and a reference membrane without an enzyme are formed on the surface of an enzyme FET and a reference FET, respectively.

solution changes, the hydrogen ion-selective membrane underlying the immobilized enzyme carriers responds to it. For precise and reliable measurement of the substrate, only the pH change produced by the enzyme-substrate reaction needs to be detected, with the measurement not being affected by the background pH change. As shown in Fig. 13, a reference FET is introduced into the measuring system together with the enzyme-immobilized FET, and the differential measurement is carried out to cancel out the background pH change. A proton-sensitive ISFET with a carrier on which enzymes are not immobilized is usually used as the reference FET. Differential measurement can detect pH changes based on the production or consumption of protons resulting from enzyme-substrate reactions by canceling out changes in pH throughout the solution, as well as changes in output due to temperature and light, as much as possible. Because the pH response characteristics and temperature characteristics of the two ISFETs are not exactly the same, noise in the measurement system cannot be completely eliminated, but it can be greatly reduced.

5.1. Penicillin. The first enzyme-immobilized FET was reported in 1980.[63] An immobilized penicillinase membrane was deposited on one of two pH-ISFETs to make a penicillin sensor. Penicillinase was immobilized by crosslinking using glutaraldehyde and albumin. The other ISFET had a membrane of only crosslinked albumin and was used as a reference FET. As penicillinase catalyzed the hydrolysis of penicillin to penicilloic acid, the local pH near the enzyme-immobilized FET shifted to a more acidic level. The response time of the sensor was about 25 s and the lifetime was 2 months with intermittent use. The dynamic range of the sensor was affected by the buffer capacity. A linear response to penicillin was obtained over a range from 0.2 to 6 mM in a 5 mM phosphate buffer at pH 7, and the upper limit of the linear range increased to 25 mM in a 20 mM phosphate buffer.

5.2. Urea. A urea sensor based on a proton-sensitive ISFET was then reported in combination with an immobilized urease membrane.[64] The immobilized urease membrane was prepared by crosslinking using urease, triacetylcellulose, 1,8-diamino-4-aminomethyloctane, and glutaraldehyde. Glycine was immobilized in the membrane of the reference FET instead of urease. The surfaces of the Si_3N_4 layers of both FETs were treated with 3-aminopropyltriethoxysilane (APTES) for better adhesion of the enzyme-immobilized and reference membranes. The differential measurement between the enzyme-immobilized and reference FETs was carried out to determine urea concentrations. On the basis of the calibration curve of the enzyme-immobilized FET, obtained in a 10 mM phosphate buffer, it was possible to determine the urea concentration over a range from 5×10^{-5} to 10^{-2} g/ml. The response time was 1 min. Responses to 1×10^{-3} g/ml urea solutions were obtained over 28 days with the data fluctuating within 3 mV at the level of 20 mV.

5.3. Glucose. A glucose sensor based on an ISFET was also reported combined with an immobilized glucose oxidase (GOD) membrane.[65] GOD was immobilized in a photosensitive polymer together with bovine serum albumin and glutaraldehyde. The pH in the solution decreased based on the GOD-glucose reaction. The response time of the sensor was 3 min and a linear relationship between the differential output and glucose concentration was obtained in the range from 0 to 300 mg/l.

5.4. Urea and glucose. A urease-immobilized FET, a GOD-immobilized FET, and a reference FET were integrated in a single chip to achieve the simultaneous detection of urea and glucose.[66),67] The layout of the chip is shown in Fig. 14(a). Three ISFETs and two MOSFETs were integrated in a single chip. Three ISFETs were used for urea, glucose, and reference FETs, respectively. Figure 14(b) shows a photograph of the fabricated chip using a silicon-on-sapphire (SOS) substrate. The orange

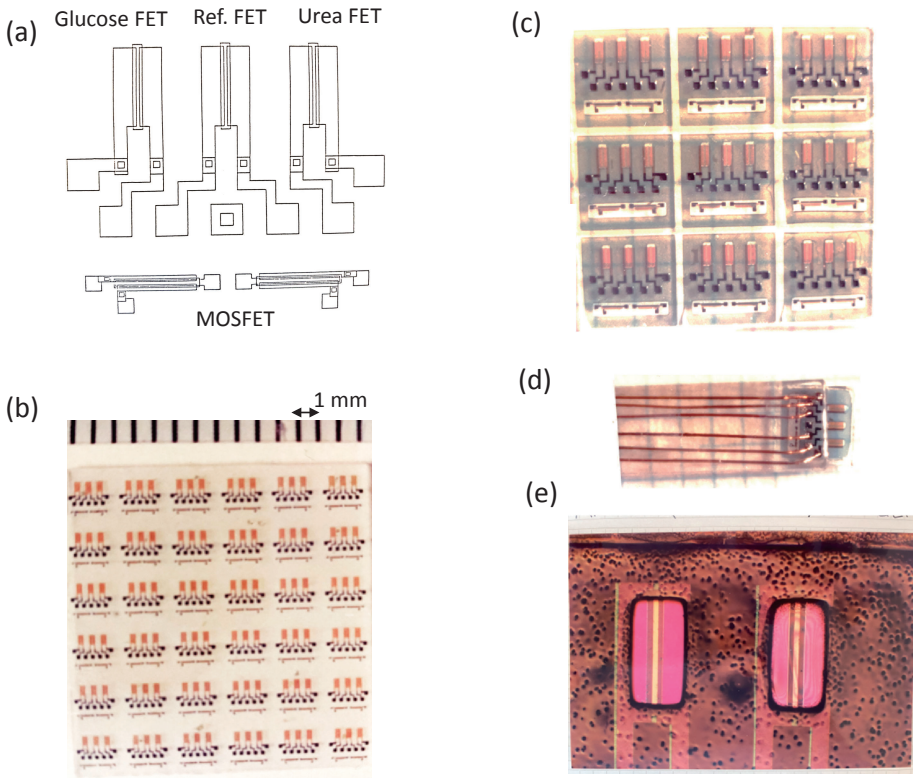

Fig. 14. Fabrication of integrated glucose and urea FETs using an SOS substrate. (a) Layout of integrated FET chip. (b) Photograph of the fabricated chip. (c) Photograph of the chips with the well structure. (d) Photograph of the chip encapsulated in epoxy resin. (e) Photograph of the immobilized enzyme membrane after drying. Reproduced from Sens. Actuators, **7**, (1985) 1–10 with permission from Elsevier.

parts are the silicon islands where the sources, drains, and channels were fabricated. The size of the chip was 2.5 mm × 2.5 mm. Because the silicon islands were surrounded entirely by the insulator, encapsulation of the SOS-FET using epoxy resin was easier compared with that of Si-FET. The well structures formed over the gate areas of the FETs for depositing different kinds of immobilized enzyme membranes separately. The photosensitive dry film with the thickness of 75 µm was used to fabricate the well structures. A photograph of the chips with the well structures is shown in Fig. 14(c). The aperture of the well structure was 200 µm × 600 µm. After wire bonding, the chip was encapsulated in epoxy resin as shown in Fig. 14(d). The stick type enzyme FET sensor was then completed and ready for use.

Photosensitive PVA was used as the immobilized enzyme membrane material for the integrated urea and glucose-sensitive FETs. The mixture of photosensitive PVA and an enzyme solution was injected into one of the well structures. A photograph of the immobilized enzyme membrane after drying is shown in Fig. 14(e). An interference fringe can be seen in the right well of the enzyme FET. A network structure of PVA was formed by the irradiation of light with a wavelength shorter than 460 nm. After photopolymerization, the enzyme was entrapped and immobilized in the network structure.[68] Because this PVA is photosensitive, it can be patterned using photolithography, but the photolithography process must be repeated as many times as the number of enzymes to be integrated. Therefore, in this experiment, urease and GOD-immobilized enzyme membranes were separately formed by dropping a small amount of photosensitive PVA containing urease or GOD into a well structure on the gate of the ISFET.

The fabricated urea and glucose FETs were immersed in a 10 mM phosphate buffer solution and 1 ml of urea or glucose solutions with various kinds of concentrations was added into the buffer solution. The output voltage changes of the glucose and urea FETs are shown in Fig. 15(a) and (b), respectively. As described in Fig. 13, the local pH in the vicinity of the gate becomes more alkaline in the urea-urease

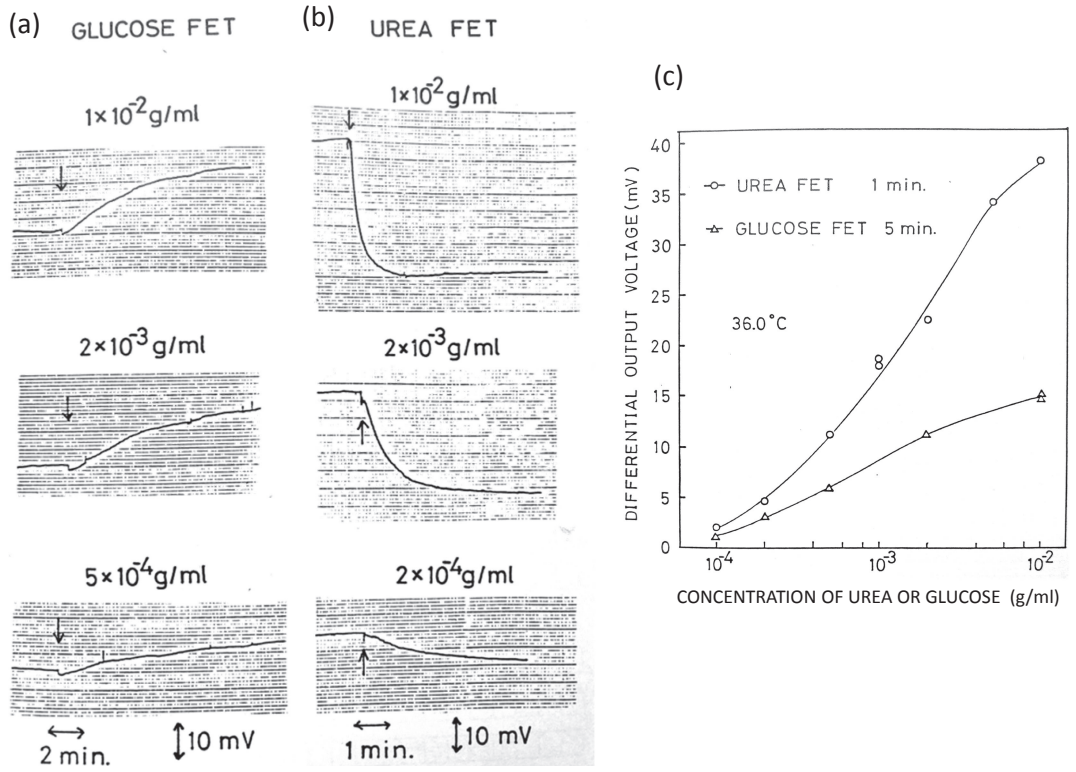

Fig. 15. Response characteristics of integrated glucose and urea FETs. (a) Responses of glucose FET to different concentrations of glucose solutions. (b) Responses of urea FET to different concentrations of urea solutions. (c) Calibration curves for glucose and urea FETs. Reproduced from Sens. Actuators, **7**, (1985) 1–10 with permission from Elsevier.

reaction, whereas it becomes more acidic in the case of the glucose-GOD reaction. Therefore, the direction of the output voltage changes was opposite between the glucose FET and urea FET. The output voltages at 5 min and 1 min after addition of glucose and urea solutions, respectively, were plotted against the concentrations of glucose and urea. The calibration curves for glucose and urea FETs are shown in Fig. 15(c). The output voltages for both glucose and urea FETs showed concentration-dependent relationships in the range from 1×10^{-4} g/ml to 1×10^{-2} g/ml. The sensitivities of both glucose and urea FETs were 8 mV/decade and 18 mV/decade, respectively, in the range from 2×10^{-4} g/ml to 2×10^{-3} g/ml. Using this approach, it was confirmed that urea and glucose concentrations can be measured independently without crosstalk.[66]

The enzymes that can be used for enzyme-immobilized FETs must be selected from those that produce or consume protons as a result of the reaction with the substrate. The enzymes used in the major enzyme-immobilized FETs reported so far include penicillinase,[63] urease,[64] glucose oxidase,[65] acetylcholinesterase,[69] lipase,[70] and DNA polymerase.[71] Enzymes are proteins, and higher-order structures unique to each enzyme play an important role in exhibiting substrate-specific catalytic activity. For an enzyme to exhibit catalytic activity in an immobilized state, the amino acid residues in the binding center and active center of the substrate should remain unchanged and the enzyme-specific higher-order structure needs to be maintained. Enzyme immobilization methods include chemical methods in which covalent bonds are formed between membrane materials and enzymes, and physical methods in which enzymes are immobilized by physical adsorption or entrapment.

5.5. Urea detection based on NH_4^+-ISFET. The activity of an enzyme is dependent on pH in the solution, and each enzyme has its own optimal pH at which its activity is maximized. Therefore, a buffer solution is usually used in the enzymatic reaction so that the enzyme-substrate reaction is performed in a solution with an optimal and constant pH. Meanwhile, the pH change produced by an enzymatic reaction is suppressed in a buffer solution and this

buffering capacity increases as the concentration of the buffer solution increases. For example, as the concentration of a phosphate buffer solution increased from 0.1 to 1 M, the response of the urease-immobilized FET decreased, while almost constant responses were obtained in phosphate buffer solutions with a concentration of 0.01 M or less.[64]

To overcome the lower sensitivity due to pH suppression in a buffer solution, ions other than hydrogen ions as products of the enzyme-substrate reaction can be used to detect the substrate. As an example, an ammonium-ion-selective membrane was used, instead of a proton-selective one, to fabricate a urea-selective FET.[72] Because ammonium ions are produced during the urea-urease reaction as described in Fig. 13, the urea concentration can be quantified by measuring the change in the ammonium ion concentration instead of the pH change. The urease-immobilized membrane was formed at the surface of the PVC-based ammonium-ion-selective membrane on the gate of the ISFET. The responses of the urea-selective FET based on the ammonium-ion-selective membrane were found not to be affected by the buffer concentration in a limited range of urea concentrations, if appropriate buffer solutions were used. However, they were affected by the selectivity of the ammonium-ion-sensitive membrane to other ions. The lower detection limit was strongly affected by the concentrations of potassium and sodium ions in the sample solution because of the insufficient selectivity of the nonactin/monactin-based ammonium-ion-selective membrane over potassium and sodium ions. A logarithmic potentiometric selectivity coefficient of an ammonium ion-selective nonactin/monactin membrane over potassium ion was -0.92.[73] This value indicated that interference by potassium ions was obtained when the potassium ion concentration was within 1 or 2 orders of magnitude higher than the ammonium ion concentration in a sample.[74] When the amount of ammonium ions locally produced in the urea-urease reaction was not sufficient, they cannot be detected with the ammonium ion selective membrane underlying the immobilized urease membrane with a background of high potassium ion concentration. In this case, the composition of the buffer solution has to be taken into consideration, just like the case with a proton-sensitive FET.

To maintain a wide dynamic range and high sensitivity as a urea sensor, the selectivity of the ion-selective membrane should be improved. Because the response of the urea-selective FET based on a proton-selective membrane is affected by the buffer capacity, the performance is difficult to improve as long as a pH-ISFET is used as a transducer in enzyme-coupled FETs. Meanwhile, the response characteristics of enzyme-coupled FETs based on an ammonium-selective membrane can be improved by improving the selectivity of the ammonium-ion-selective membrane. Therefore, this approach may be one of future directions to realize enzyme FETs without limitation of buffer capacity.

5.6. DNA. DNA exhibits specific affinity to complementary DNA even for a short fragment of about 20 bases (6.8 nm), and, therefore, molecular recognition reactions such as hybridization can be carried out within the Debye length range. Because double-stranded DNA after hybridization has high affinity at a controlled temperature, the capture-reaction step and the detection step can be separated, unlike in the measurement of ions. In many DNA analyses, after hybridization, a washing step is conducted, and separation of bound and free targets (B/F separation) is performed before the detection process. As with conventional DNA chips/DNA microarrays, the products of polymerase chain reaction (PCR) amplification after nucleic acid extraction are used as samples for FET-based DNA analyses. Therefore, they do not contain interfering substances such as proteins, and potentiometric measurements can be performed in a controlled environment to some extent. Therefore, it is practical to control the Debye length using a diluted buffer solution when the changes in negative charges based on phosphate groups of DNA after molecular recognition are detected with FETs modified with DNA probes. Not only hybridization but also the binding reaction between DNA probes and DNA binders,[75] and the primer extension reaction were designed on the surface of the gate of DNA-modified FETs for analyses of single-nucleotide polymorphism (SNP) and DNA sequencing.

5.7. Genotyping. The base sequence of the DNA probe was designed so that the 5′ end was immobilized on the surface of the gate insulator and the 3′ end served as the SNP site. After hybridization between the probe DNA and target DNA, if the SNP site is complementary, a polynucleotide is synthesized by the introduction of thermostable Taq DNA polymerase together with deoxynucleotide triphosphates (dNTPs). Because the charge density at the gate surface increases as a result of synthesis of polynucleotides, the threshold voltage of the FET changes and the event of the primer extension

reaction can be detected.[76] SNP genotyping is based on the sequence-specific primer extension of two allele-specific oligonucleotide probes that differ at their 3′ end nucleotide defining the alleles. Normal oligonucleotide probes with a base sequence complementary to a wild-type sample were immobilized on the gate surface of one FET (N-type FET), whereas mutant oligonucleotide probes with a base sequence complementary to a mutant sample were immobilized on the gate surface of another FET (M-type FET). The target DNA was hybridized with the normal and mutant oligonucleotide probes (11 bases) on the gate surface of each FET. It was difficult to distinguish a single base difference based on just hybridization. So, the hybridization events were followed by the introduction of DNA polymerase and all four deoxynucleotides. The sequence-specific elongation may be controlled by a match or mismatch at the 3′ end of each oligonucleotide probe. When the 3′ end of the oligonucleotide probe was complementary to the polymorphic site of the target DNA, DNA polymerase extended the immobilized oligonucleotide probes with dNTPs in a template-dependent manner. As a result of the elongation reaction, negative charges increased at the gate surface of the FET because of intrinsic negative charges of the polynucleotide. This change in charge density can be detected as a shift in the threshold voltage of the FET. Meanwhile, when the 3′ end of the oligonucleotide probe was not complementary to the target DNA, an elongation reaction did not occur and the charges at the gate surface did not change. Thus, information on match or mismatch at the polymorphic site of the target DNA can be detected by using the DNA-immobilized FET, which allowed simple and precise discrimination of SNP genotypes. As samples for the genotyping experiments, three different genotypes using synthetic oligonucleotides for the −122 locus of the factor VII gene were prepared. The N-type and M-type FETs were set in a buffer solution and hybridized with a normal/normal (n/n) homozygote sample, a normal/mutant (n/m) heterozygote sample, and a mutant/mutant (m/m) homozygote sample. After introducing the FETs into the incubated reaction mixture including thermostable DNA polymerase and dNTPs, the differential threshold voltage shifts were evaluated. The ratios of the differential threshold voltage shifts between the N-type and M-type FETs were 9.96, 1.11, and 0.08 for the n/n homozygote, n/m heterozygote, and m/m homozygote samples, respectively. It turned out that DNA-immobilized FETs were effective for SNP typing because they can discriminate with high accuracy the presence or absence of elongation reactions caused by differences in bases at SNP sites.

5.8. DNA sequencing. In the primer extension reaction on the gate insulator of the FET, each dNTP, that is, deoxyadenosine triphosphate, deoxyguanosine triphosphate, deoxycytidine triphosphate, or deoxythymidine triphosphate, was separately added sequentially together with Taq DNA polymerase, as shown in Fig. 16, and the threshold voltage change of the DNA-immobilized FET was measured in a phosphate buffer solution (0.025 M) after washing the FETs.[77] If the added dNTP was complementary to the base of the target DNA, only one base was synthesized by the extension reaction, and if it was not complementary, the synthesis reaction did not occur. Therefore, the unknown base sequence of the target DNA can be analyzed by measuring the change in the threshold voltage. The cycle of single-base extension and measurement of the V_T was repeated iteratively to determine the base sequence of the target DNA. Three examples of DNA sequencing based on intrinsic molecular charges are shown in Fig. 17.[78] When the base sequence of the R353Q region of the factor VII gene was used as the target DNA, the V_T shifted in a positive direction only after single-base extension with the specific deoxynucleotides that were complementary to the base sequence of the target DNA. The change in V_T for three-base extension, GGG, was 6.9 mV, which was larger than that for one-base extension, but was not three times as expected from the number of intrinsic charges.[77] Notably, the measured V_T shift was 3.2 mV on average for single-base extensions; the resulting probe density at the gate surface was $7.3 \times 10^{11}\,\mathrm{cm}^{-2}$. It is important to detect single-base extension quantitatively to reduce the base-call error, especially for continuous sequences of the same base. The density and orientation of the immobilized oligonucleotide probes have to be controlled during a series of extension reactions at 72 °C. It is a more effective and practical to use a modified nucleotide with a reversible blocking group called a "reversible terminator" instead of dNTPs. The blocking group can be removed chemically for the next single-base extension reaction. Using a reversible terminator, a single-base synthesis can proceed one by one even for continuous sequences of the same base, which leads to more precise DNA sequencing. Using the sequencing method based on ISFETs, an electrical DNA sequencing system has been developed by Ion

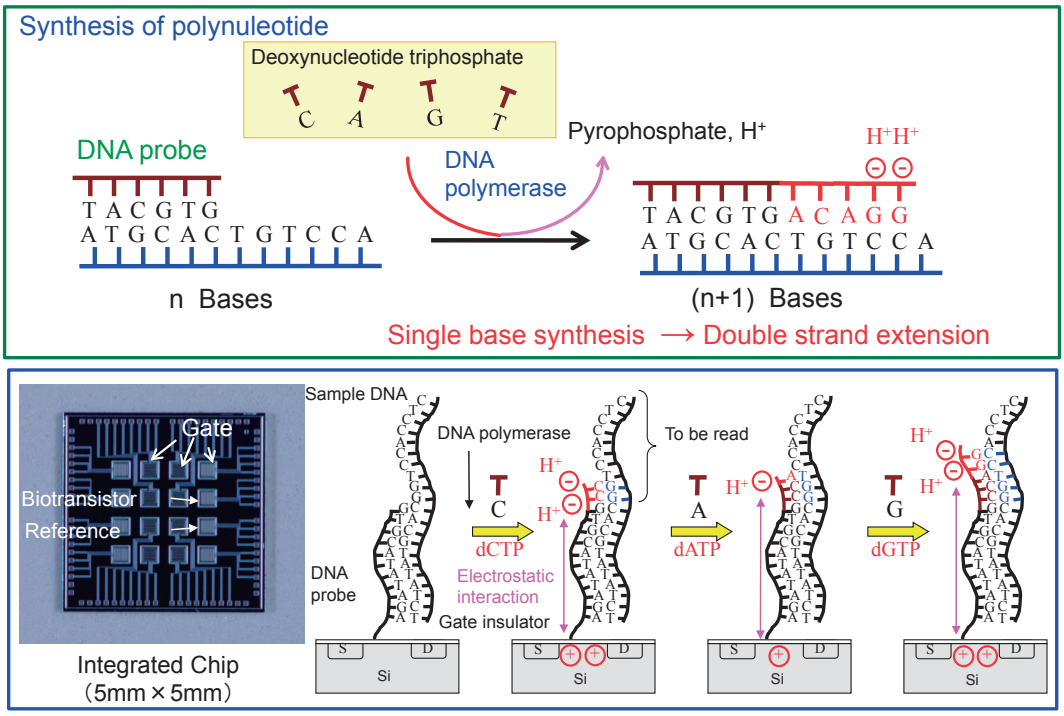

Fig. 16. Design of single-base extension reaction on the gate surface of the FET. Reproduced from Angew. Chem. Int. Ed., **45**, (2006) 2225–2228 with permission from John Wiley and Sons.

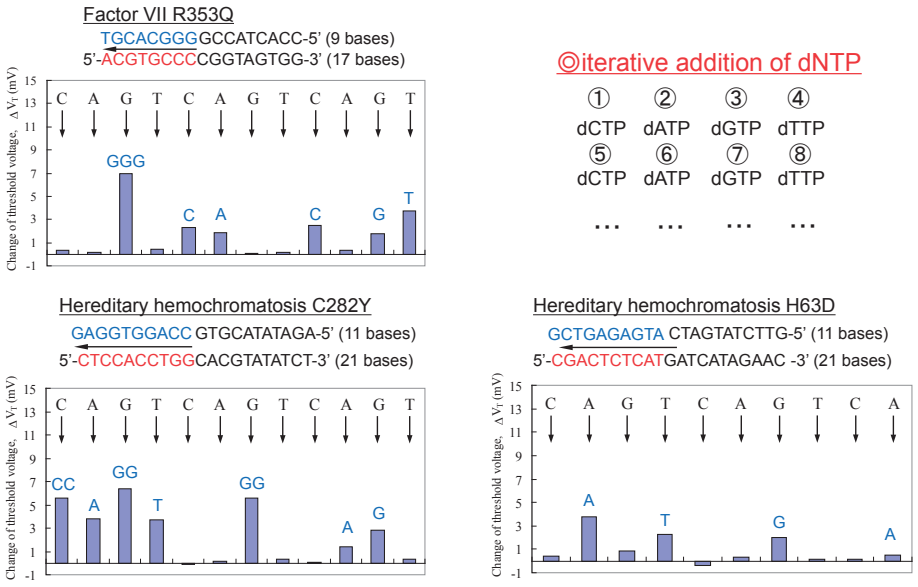

Fig. 17. Examples of DNA sequencing based on intrinsic molecular charges. Reproduced from Angew. Chem. Int. Ed., **45**, (2006) 2225–2228 with permission from John Wiley and Sons.

Torrent using advanced semiconductor technologies.[7] A large-scale array of 1.5 million ISFETs was integrated with signal processing circuits in a 10 × 10 mm^2 chip, which was mounted in a flow cell. Up to 20 million bases could be analyzed per run. Primers and DNA polymerase were bound to template-carrying beads and the beads were then loaded into wells arrayed on the semiconductor chip. In this

system, the pH change caused by primer extension was detected by the ISFET on the bottom of each well. The system performance was demonstrated through whole-genome sequencing of bacterial genomes. This is the first example of commercialized DNA-immobilized FETs for analyzing DNA sequences with high speed and high throughput.

5.9. Liberated proteins. Enzyme-linked immunosorbent assays (ELISAs) are commonly used to detect biomarkers such as proteins. In this technology, an antigen-antibody reaction is carried out on a substrate, and the target antigen is detected by generating optically detectable products through the reaction of the enzyme bound to the secondary antibody and the substrate. Horseradish peroxidase and alkaline phosphatase, among others, are usually used as enzymes for optical detection. Recently, a proton ELISA was reported using proton-sensitive ISFET in combination with GOD, which was attached to the secondary antibody.[79] An antigen-antibody reaction was carried out on the surface of the sensing region of the ISFET. The surface of the pH-sensitive membrane of the ISFET was treated with aminosilane to introduce amino groups onto the surface, and the primary antibody (capture antibody) was immobilized using glutaraldehyde. After the antigen to be detected was specifically bound to the primary antibody, it was reacted with a biotin-modified secondary antibody (detection antibody) to construct a sandwich structure. Glucose oxidase, in contrast, was conjugated to avidin, and the avidin-biotin bond was used to conjugate glucose oxidase to the secondary antibody. Similar to the conventional ELISA, when the antigen is present in the sample, it binds to the capture antibody in the sensing region of the pH-sensitive ISFET, and then when the detection antibody conjugated with GOD is introduced, it specifically binds to the antigen. Therefore, glucose oxidase is bound to the pH sensing region depending on the amount of antigen. When the substrate glucose is introduced into the sensing region, protons are generated in accordance with the amount of glucose oxidase. The antigen concentration is quantified by detecting the protons produced. On the basis of this method, C-reactive protein (CRP) was detected. A biotinylated anti-CRP antibody was used as the detection antibody, and a 25 mM KCl aqueous solution was used as the measurement solution to eliminate the buffering effect. Real-time measurement of CRP was performed by proton ELISA in these conditions, and CRP at a concentration of 25 pg/mL was detectable. Because binding between the antigen and antibody was strong, one of the problems was that the ISFET chip can only be used for one measurement because the capture antibody was directly immobilized on the sensing area of the ISFET. By combining the ISFET and ELISA detection schemes, the antigen-antibody reaction can be detected without depending on the Debye length.

5.10. Live cell assay of membrane proteins (cell-based FET). Not only biomolecules but also cells can be placed on the gate surface of the ISFETs.[77),80)–85)] A novel strategy for epidermal growth factor receptor (EGFR) detection using a cell-based FET with enzymatic chemical signal amplification has been proposed.[86)] Among potential biomarkers for cancer diagnosis in liquid biopsy, circulating tumor cells (CTCs) and extracellular vesicles (EVs) have membrane proteins that carry molecular information on the biological process through the metastatic cascade. The binding affinity between molecular probes and surface proteins expressed on CTCs is used for the capture and detection of CTCs. Epithelial cell adhesion molecule (EpCAM) is used as a specific biomarker in most positive selection methods for CTCs, including the CellSearch system, which has been approved by the United States Food and Drug Administration. While in the circulation, membrane proteins may change throughout tumor progression. CTCs undergo epithelial–mesenchymal transition (EMT) and, as a result, the expression of epithelial markers, including EpCAM, decreases, and the expression of mesenchymal markers, such as vimentin, increases. Therefore, both epithelial and mesenchymal markers should be detected simultaneously to elucidate the mechanism by which metastasis proceeds.

The detection scheme using the cell-based FET is shown in Fig. 18. The system consists of an ISFET, a capture material layer, cells, anti-EGFR antibody, and secondary antibody with GOD.[87)] When a glucose solution is added to the surface of the cell-based FET, the local pH near the surface of the cells changes, depending on the expression level of EGFR (as a result of a GOD-glucose reaction). In this scheme, extracellular matrix (ECM) gel was formed on the surface of the ISFET as a capture material layer. Cells are nonspecifically captured on the surface of the ECM gel, so that the cells to be analyzed are independent of expression of the specific antigens. Antibodies conjugated with an enzyme are then specifically bound to surface antigens to

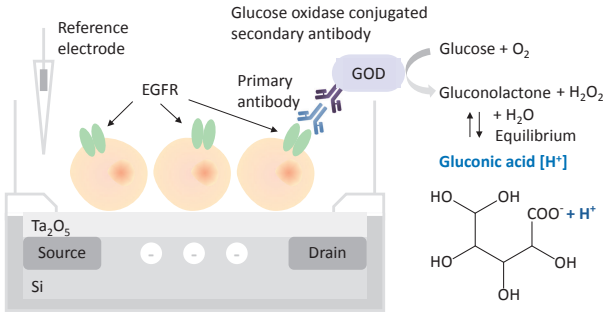

Fig. 18. Principle of detecting EGFR via enzymatic chemical signal amplification using ISFET. Reprinted with permission from J. Am. Chem. Soc., **144**, (2022) 16545–16552. Copyright 2022 American Chemical Society.

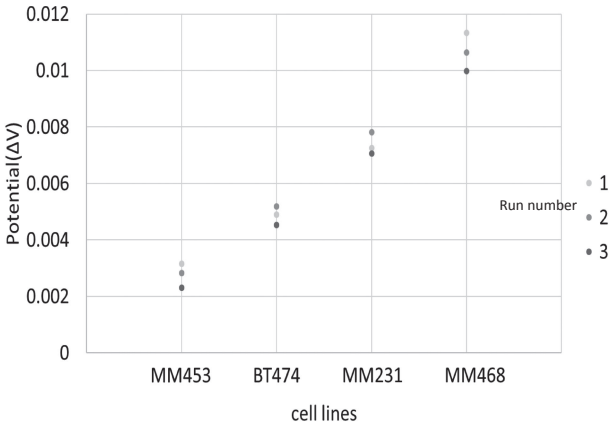

Fig. 19. Comparison of potential changes based on glucose-GOD reactions among MM453, BT474, MM231, and MM468. Reprinted with permission from J. Am. Chem. Soc., **144**, (2022) 16545–16552. Copyright 2022 American Chemical Society.

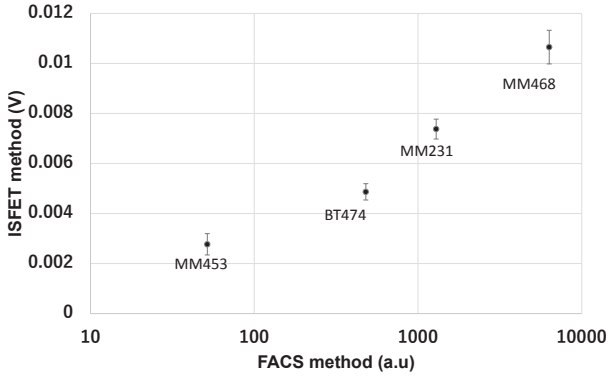

Fig. 20. Correlation between fluorescence intensity using a FACS method and potential change using an ISFET method (n = 3). Reprinted with permission from J. Am. Chem. Soc., **144**, (2022) 16545–16552. Copyright 2022 American Chemical Society.

characterize the phenotypes of the cells. Upon addition of the substrate for the enzyme, local pH changes are generated on the surface of the FET depending on the expression level of the surface antigen. If multiple antibodies conjugated with different enzymes, which should induce local pH change as a result of reactions with their substrates, are bound to the surface antigens, multiple antigens can be detected by sequential addition of the respective substrates.[88] In the experiment, four human breast cancer cell lines (BT474, MM231, MM468, and MM453) were used as a model for CTC to compare the expression levels of EGFR. The expression levels of EGFR among the four cell lines were determined using fluorescence-activated cell sorting (FACS) in addition to the cell-based FETs. The fluorescence intensity of MM468 was the highest among the four cell lines. MM231 showed the second highest intensity, followed by BT474, and MM453 showed the lowest intensity. Each cell line was seeded onto the ECM gel-coated ISFETs, and an anti-EGFR antibody and secondary antibody conjugated to GOD were subsequently applied to the cell surfaces. Then, after optimization of the glucose concentration, 10 mM glucose solution was added to the reaction chamber of each cell-based FET, and the potential changes in response to the glucose-GOD enzymatic reaction were monitored. The potential shifts in 10 min after the addition of glucose were compared among the four cell lines, as shown in Fig. 19. The size of the potential shift (ΔV) was in the order MM468 > MM231 > BT474 > MM453, which reflected the order of the expression levels of EGFR. This tendency was consistent with the EGFR expression level analyzed by FACS. Figure 20 shows a comparison of EGFR expression levels measured by the ISFET method and the FACS method. A good correlation can be obtained between the pH values measured with the cell-based FETs and the fluorescence intensities measured with the FACS, showing a correlation coefficient of 0.976.

The sizes of the cells are in the order of a few tens of micrometers, and, therefore, a single cell can be placed on the surface of a single gate of the FET. Selective capture of the cells could be realized based on hydrophobic/hydrophilic control of the gate surface.[86),89] Using single-cell-based FETs, the number of cells that have higher expression of specific antigens on the cell membranes can be counted. This method can be applied to detect surface antigens

on the membranes of EVs. Although the size of an EV is approximately two orders of magnitude smaller than that of a cell, it is technically possible to fabricate the gate of an FET whose size is comparable to that of an EV. Therefore, a single EV could be captured on a single gate of a nanoscale FET. EVs are contained in bodily fluids such as urine and saliva, and EV samples can be collected in a noninvasive or minimally invasive manner.

6. Conclusion and future perspectives

More than 50 years have passed since the first ISFET was reported by P. Bergveld in 1970. Since then, significant progress has been achieved in the field of solid-state biosensors. Various sensing devices with high-density integration and flexible configuration, as well as new applications for clinical diagnosis and healthcare, have been developed using blood, serum, and other bodily fluids such as sweat, tears, and saliva. Intensive research on the working principle, the gate materials, and the drift mechanism during the early stage led to the commercialization of a discrete pH-sensitive ISFET for laboratory use. With the need to process a large amount of biological information, a high-density array of ISFET was developed by exploiting the advantages of advanced semiconductor technologies, and commercialized in combination with an enzymatic primer extension reaction as a DNA sequencer in 2011. Accurate detection of the target molecule is crucial not only for early diagnosis and prognosis but also for healthcare and the noninvasive monitoring of biomarkers. As described in this review, different types of materials, such as inorganic materials, metals, polymers, and biomolecules, are mixed together on the surface of the gate while maintaining their own functions; therefore, compatibility among different materials has to be optimized so that the best detection performance of solid-state biosensors, including stability and reliability, is achieved as designed.

In the field of medical treatment and diagnosis, technologies to acquire biometric information noninvasively and without constraints have attracted attention. However, our ability to obtain biological and medical information by external physiological monitoring, to realize preemptive medicine, early diagnosis, and healthcare, is currently limited. Through liquid biopsy, it is possible to collect samples in noninvasive and minimally invasive ways, using bodily fluids such as urine and saliva as samples, in addition to blood.[90)–92)] EVs and exosomes by themselves or miRNAs in exosomes are attracting attention as promising biomarkers for minimally invasive clinical testing in non-hospital settings, such as a physician's office or patient's home, because EVs, exosomes, and miRNAs are present in urine and saliva. Solid-state biosensors are suitable for the rapid, cost-effective, and noninvasive identification of biomarkers at various timepoints during a disease's course. The development of a new platform for detecting circulating free DNA, circulating tumor DNA, miRNAs, EVs, and exosomes is at the forefront of efforts to demonstrate the effectiveness of liquid biopsy for disease diagnosis as well as prognosis, early diagnosis, preemptive medicine, and healthcare.

In the semiconductor industry, the limit of miniaturization of transistors has been pointed out, and research aimed at diversification has also been conducted in parallel with research in pursuit of the limit of miniaturization. As one direction for such diversification, the integration of semiconductor devices and biotechnology is being considered. A solid-state biosensor is one such concrete example for the medical and life sciences. It will also be applied to information processing devices that directly use tissues, cells, and biomolecules in combination with semiconductor devices in the future. In semiconductor devices, electrons (and holes) serve as carriers of information, and the flow of information is controlled by p-n junctions and field effects in semiconductor crystals. Electrons can be carriers of information because they have electric charges. However, ions can also serve as information carriers because they have electric charges. Unlike electrons, ions have characteristics such as positive/negative charge, valence, and mass, and various properties such as the potential for using electrode reactions on the surface of metal electrodes and equilibrium reactions at interfaces between different materials for signal processing. In addition, ions in an ionic conductor generally diffuse more slowly than electrons in a solid. We have proposed the use of ions in addition to electrons as carriers of information.[93)] By controlling ion transport in materials using redox reactions and equilibrium reactions involving ions, it would be possible to realize characteristics and functions that cannot be achieved with conventional semiconductor materials such as silicon. We believe that information processing devices can be created, and that a new research field called "iono-electronics" will be established. We have already reported a sensor device[94),95)] that combines a field effect transistor with a solid electrolyte, and a chemo-mechanical signal conver-

sion device[61] that uses a polymer gel on a field effect transistor. In addition, similar studies such as on an "ion circuit" using polymer electrolyte,[96] cell culture by an electrochemical transistor using conductive polymer,[97] and an "atomic switch" using the deposition and dissolution of solid electrolyte[98] have recently been reported. We hope that these studies will develop further in the future to reinforce the new trend of "iono-electronic" devices.[99),100]

Acknowledgments

We would like to thank all the members of our laboratories and collaborators for their support. We are also grateful to the colleagues who contributed to the original studies cited in this review. This work was supported in part by CREST "Creation of Nanosystems with Novel Functions through Process Integration" and the Center of Innovation (COI) Program (JPMJCE1305) from Japan Science and Technology Agency (JST), and by grant-in-aid for Scientific Research on Innovative Areas "Molecular Soft-Interface Science" and the Nanotechnology Platform Program (JPMXP09F12NM0064) from Ministry of Education, Culture, Sports, Science and Technology (MEXT).

References

1) Bergveld, P. (1970) Development of an ion-sensitive solid-state device for neurophysiological measurements. IEEE Trans. Biomed. Eng. **BME-17**, 70–71.
2) Terry, S.C., Hermann, J.H. and Angel, J.B. (1979) A gas chromatographic air analyzer fabricated on a silicon wafer. IEEE Trans. Electron Dev. **26**, 1880–1886.
3) Miyahara, Y., Matsu, F., Shiokawa, S., Moriizumi, T., Matsuoka, H., Karube, I. *et al.* (1983) Biosensor using anisotropic etching technique of Si. *In* Proceedings of the 3rd Sensor Symposium (Tsukuba, Japan, 1983), pp. 21–26.
4) Manz, A., Miyahara, Y., Miura, J., Watanabe, Y., Miyagi, H. and Sato, K. (1990) Design of an open-tubular column liquid chromatograph using silicon chip technology. Sens. Actuat. B **1**, 249–255.
5) Fodor, S.P.A., Read, J.L., Pirrung, M.C., Stryer, L., Lu, A.T. and Solas, D. (1991) Light-directed, spatially addressable parallel chemical synthesis. Science **251**, 767–773.
6) Rothberg, J., Hinz, W., Rearick, T., Schultz, J., Mileski, W., Davey, M. *et al.* (2011) An integrated semiconductor device enabling non-optical genome sequencing. Nature **475**, 348–352.
7) Tabata, M. and Miyahara, Y. (2019) Liquid biopsy in combination with solid-state electrochemical sensors and nucleic acid amplification. J. Mater. Chem. B **7**, 6655–6669.
8) Tabata, M. and Miyahara, Y. (2022) From new materials to advanced biomedical applications of solid-state biosensor: A review. Sensor. Actuat. B **352**, 131033.
9) Zdrachek, E. and Bakker, E. (2019) Potentiometric sensing. Anal. Chem. **91**, 2–26.
10) Labib, M., Sargent, E.H. and Kelley, S.O. (2016) Electrochemical methods for the analysis of clinically relevant biomolecules. Chem. Rev. **116**, 9001–9090.
11) Várguez, P.E.M., Brunel, F. and Raimundo, J.-M. (2020) Recent Electrochemical/electrical microfabricated sensor devices for ionic and polyionic analytes. ACS Omega **5**, 4733–4742.
12) Ding, J. and Qin, W. (2020) Recent advances in potentiometric biosensors. Trends Analyt. Chem. **124**, 115803.
13) Sakata, T. (2019) Biologically coupled gate field-effect transistors meet in vitro diagnostics. ACS Omega **4**, 11852–11862.
14) Bandodkar, A.J., Jeerapan, I. and Wang, J. (2016) Wearable chemical sensors: Present challenges and future prospects. ACS Sens. **1**, 464–482.
15) Mayer, M., Baeumner, A.J. and Megatrend, A. (2019) Challenging analytical chemistry: Biosensor and chemosensor concepts ready for the internet of things. Chem. Rev. **119**, 7996–8027.
16) Cattrall, R.W. and Freiser, H. (1971) Coated wire ion-selective electrodes. Anal. Chem. **43**, 1905–1906.
17) Moss, S.D., Janata, J. and Johnson, C.C. (1975) Potassium ion-sensitive field effect transistor. Anal. Chem. **47**, 2238–2243.
18) Freiser, H. (1980) Coated wire ion-selective electrodes. *In* Ion-selective Electrodes in Analytical Chemistry (ed. Freiser, H.). Plenum Press, New York, pp. 85–105.
19) Cattrall, R.W. and Hamilton, I.C. (1984) Coated-Wire Ion-Selective Electrodes. Ion-Selective Electrode Rev. **6**, 125–172.
20) Janata, J. and Huber, R.J. (1980) Chemically sensitive field effect transistors. *In* Ion-selective Electrodes in Analytical Chemistry (ed. Freiser, H.). Plenum Press, New York, pp. 107–174.
21) van den Vlekkert, H., Francis, C., Grisel, A. and de Rooij, N. (1988) Solvent polymeric membranes combined with chemical solid-state sensors. Analyst **113**, 1029–1033.
22) Miyahara, Y. and Simon, W. (1991) Comparative studies between ion-selective field effect transistors and ion-selective electrodes with polymeric membranes. Electroanalysis **3**, 287–292.
23) Maj-zurawska, M. and Hulanicki, A. (1982) Effect of the platinum surface on the potential of nitrate-selective electrodes without internal solution. Anal. Chim. Acta **136**, 395–398.
24) Cattrall, R.W., Drew, D.M. and Hamilton, I.C. (1975) Some alkylphosphoric acid esters for use in coated-wire calcium-selective electrodes: Part I. Response characteristics. Anal. Chim. Acta **76**, 269–277.

25) Hulanicki, A. and Trojanowicz, M. (1976) Calcium-selective electrodes with PVC membranes and solid internal contacts. Anal. Chim. Acta **87**, 411–417.
26) Fogt, E.J., Untereker, D.F., Norenberg, M.S. and Meyerhoff, M.E. (1985) Response of ion-selective field effect transistors to carbon dioxide and organic acids. Anal. Chem. **57**, 1995–1998.
27) Smith, M.D., Genshaw, M.A. and Greyson, J. (1973) Miniature solid state potassium electrode for serum analysis. Anal. Chem. **45**, 1782–1784.
28) Sudhölter, E.J.R., van der Wal, P.D., Skowronska-Ptasinska, M., van den Berg, A., Bergveld, P. and Reinhoudt, D.N. (1990) Modification of ISFETs by covalent anchoring of poly(hyroxyethyl methacrylate) hydrogel. Introduction of a thermodynamically defined semiconductor-sensing membrane interface. Anal. Chim. Acta **230**, 59–65.
29) Morf, W.E. (1981) The Principles of Ion-Selective Electrodes and of Membrane Transport. Akademiai Kiado, Budapest.
30) Janata, J. (1994) Historical review. Twenty years of ion-selective field-effect transistors. Analyst **119**, 2275–2278.
31) Miyahara, Y., Yamashita, K., Ozawa, S. and Watanabe, Y. (1996) Shift and drift of electromotive forces of solid-state electrode with ion-selective liquid membranes. Anal. Chim. Acta **331**, 85–95.
32) Zou, X.U., Zhen, X.V., Cheong, J.H. and Bühlmann, P. (2014) Calibration-free ionophore-based ion-selective electrodes with a Co(II)/Co(III) redox couple-based solid contact. Anal. Chem. **86**, 8687–8692.
33) Anderson, E.L., Chopade, S.A., Spindler, B., Stein, A., Lodge, T.P., Hillmyer, M.A. *et al.* (2020) Solid-contact ion-selective and reference electrodes covalently attached to functionalized poly(ethylene terephthalate). Anal. Chem. **92**, 7621–7629.
34) Gao, W., Ota, H., Kiriya, D., Takei, K. and Javey, A. (2019) Flexible electronics toward wearable sensing. Acc. Chem. Res. **52**, 523–533.
35) Sonner, Z., Wilder, E. and Heikenfeld, J. (2015) The microfluidics of the eccrine sweat gland, including biomarker partitioning, transport, and biosensing implications. Biomicrofluidics **9**, 031301.
36) Henry, C. (1996) Product Review: Measuring the Masses: Quartz crystal microbalances. Anal. Chem. **68**, 625A–628A.
37) Handley, J. (2001) Product Review: Quartz Crystal Microbalances. Anal. Chem. **73**, 225A–229A.
38) Frutos, A.G. and Corn, R.M. (1998) Peer Reviewed: SPR of Ultrathin Organic Films. Anal. Chem. **70**, 449A–455A.
39) Zubritsky, E. (2000) Product Review: New choices for SPR. Anal. Chem. **72**, 289A–292A.
40) Tabata, M., Kataoka-Hamai, C., Nogami, K., Tsuya, D., Goda, T., Matsumoto, A. *et al.* (2021) Organic and inorganic mixed phase modification of silver surface for functionalization with biomolecules and stabilization of electromotive force. RSC Advances **11**, 24958–24967.
41) Ulman, A. (1996) Formation and structure of self-assembled monolayers. Chem. Rev. **1996**, 1533–1544.
42) Wasserman, S.R., Tao, Y.T. and Whitesides, G.M. (1989) Structure and reactivity of alkylsiloxane monolayers formed by reaction of alkyltrichlorosilanes on silicon substrates. Langmuir **5**, 1074–1087.
43) Ishida, H., Chiang, C.H. and Koenig, J.L. (1982) The structure of aminofunctional silane coupling agents: 1. γ-Aminopropyltriethoxysilane and its analogues. Polymer **23**, 251–257.
44) Silberzan, P., Léger, L., Ausserré, D. and Benattar, J.J. (1991) Silanation of silica surfaces. A new method of constructing pure or mixed monolayers. Langmuir **7**, 1647–1651.
45) Angst, D.L. and Simmons, G.W. (1991) Moisture absorption characteristics of organosiloxane self-assembled monolayers. Langmuir **7**, 2236–2242.
46) Kallury, K.M.R., Macdonald, P.M. and Thompson, M. (1994) Effect of surface water and base catalysis on the silanization of silica by (aminopropyl)alkoxysilanes studied by X-ray photoelectron spectroscopy and 13C cross-polarization/magic angle spinning nuclear magnetic resonance. Langmuir **10**, 492–499.
47) Fadeev, A.Y. and McCarthy, T.J. (2000) Self-assembly is not the only reaction possible between alkyltrichlorosilanes and surfaces: monomolecular and oligomeric covalently attached layers of dichloro- and trichloroalkylsilanes on silicon. Langmuir **16**, 7268–7274.
48) Acres, R.G., Ellis, A.V., Alvino, J., Lenahan, C.E., Khodakov, D.A., Metha, G.F. *et al.* (2012) Molecular structure of 3-aminopropyltriethoxysilane layers formed on silanol-terminated silicon surfaces. J. Phys. Chem. C **116**, 6289–6297.
49) Brittain, W.J., Brandsetter, T., Prucker, O. and Rühe, J. (2019) The surface science of microarray generation–A critical inventory. ACS Appl. Mater. Interfaces **11**, 39397–39409.
50) Laibinis, P.E., Whitesides, G.M., Allara, D.L., Tao, Y.T., Parikh, A.N. and Nuzzo, R.G. (1991) Comparison of the structures and wetting properties of self-assembled monolayers of n-alkanethiols on the coinage metal surfaces, copper, silver, and gold. J. Am. Chem. Soc. **113**, 7152–7167.
51) Holmlin, R.E., Chen, X.X., Chapman, R.G., Takayama, S. and Whitesides, G.M. (2001) Zwitterionic SAMs that resist nonspecific adsorption of protein from aqueous buffer. Langmuir **17**, 2841–2850.
52) Goda, T., Masuno, K., Nishida, J., Kosaka, N., Ochiya, T., Matsumoto, A. *et al.* (2012) A label-free electrical detection of exosomal microRNAs using microelectrode array. Chem. Commun. **48**, 11942–11944.
53) Goda, T., Singi, A.B., Maeda, Y., Matsumoto, A., Torimura, M., Aoki, H. *et al.* (2013) Label-free potentiometry for detecting DNA hybridization using peptide nucleic acid and DNA probes.

Sensors **13**, 2267–2278.
54) Kesler, V., Murmann, B. and Soh, H.T. (2020) Going beyond the Debye length: Overcoming charge screening limitations in next generation bioelectronic sensors. ACS Nano **14**, 16194–16201.
55) Jayasena, S.D. (1999) Aptamers: An emerging class of molecules that rival antibodies in diagnostics. Clin. Chem. **45**, 1628–1650.
56) Goda, T. and Miyahara, Y. (2012) A hairpin DNA aptamer coupled with groove binders as a smart switch for a field-effect transistor biosensor. Biosens. Bioelectron. **32**, 244–249.
57) Matsumoto, A., Sato, N., Sakata, T., Yoshida, R., Kataoka, K. and Miyahara, Y. (2009) Chemical-to-electrical-signal transduction synchronized with smart gel volume phase transition. Adv. Mater. **21**, 4372–4378.
58) Kataoka, K., Miyazaki, H., Bunya, M., Okano, T. and Sakurai, Y. (1998) Totally synthetic polymer gels responding to external glucose concentration: Their preparation and application to on–off regulation of insulin release. J. Am. Chem. Soc. **120**, 12694–12695.
59) Matsumoto, A., Ikeda, S., Harada, A. and Kataoka, K. (2003) Glucose-responsive polymer bearing a novel phenylborate derivative as a glucose-sensing moiety operating at physiological pH conditions. Biomacromolecules **4**, 1410–1416.
60) Maeda, Y., Matsumoto, A., Miura, Y. and Miyahara, Y. (2012) Preparation of alpha-mannoside hydrogel and electrical detection of saccharide-protein interactions using the smart gel-modified gate field effect transistor. Nanoscale Res. Lett. **7**, 108.
61) Matsumoto, A., Endo, T., Yoshida, R. and Miyahara, Y. (2009) Electrically visualized chemo-mechanical signal transduction by using a smart gel gate-modified field effect transistor. Chem. Commun. 5609–5611.
62) Miyahara, Y., Shiokawa, S., Moriizumi, T., Matsuoka, H., Karube, I. and Suzuki, S. (1982) Biosensor using ISFET with immobilized enzyme membrane. *In* Proceedings of the 2nd Sensor Symposium. The Institute of Electrical Engineers of Japan, 1982, pp. 91–95.
63) Caras, S. and Janata, J. (1980) Field effect transistor sensitive to penicillin. Anal. Chem. **52**, 1935–1937.
64) Miyahara, Y., Moriizumi, T., Matsuoka, H., Karube, I. and Suzuki, S. (1983) Micro urea sensor using semiconductor and enzyme-immobilization technologies. J. Chem. Soc. Jpn. 823–830 (in Japanese with English abstract).
65) Hanazato, Y. and Shiono, S. (1983) Bioelectrode using two hydrogen ion sensitive field effect transistors and a platinum wire pseudo reference electrode. *In* Proceedings of International Meeting on Chemical Sensors, Fukuoka, Japan, 1983. Analytical Chemistry Symposia Series, Vol. 17, Elsevier, pp. 513–518.
66) Miyahara, Y., Moriizumi, T. and Ichimura, K. (1985) Integrated enzyme FETs for simultaneous detections of urea and glucose. Sens. Actuators **7**, 1–10.
67) Shiono, S., Hanazato, Y. and Nakako, M. (1986) Urea and glucose sensors based on ion sensitive field effect transistor with photolithographically patterned enzyme membrane. Anal. Sci. **2**, 517–521.
68) Ichimura, K. (1984) A convenient photochemical method to immobilized enzymes. J. Polym. Sci.: Polym. Chem. Ed. **22**, 2817–2828.
69) Miyahara, Y., Matsu, F., Moriizumi, T., Matsuoka, H., Karube, I. and Suzuki, S. (1983) Micro enzyme sensors using semiconductor and enzyme-immobilization techniques. *In* Proceedings of International Meeting on Chemical Sensors, Fukuoka, Japan, 1983. Analytical Chemistry Symposia Series, Vol. 17, Elsevier, pp. 501–506.
70) Hanazato, Y., Nakako, M., Shiono, S. and Maeda, M. (1989) Integrated multi-biosensors based on an ion-sensitive field-effect transistor using photolithographic techniques. IEEE Trans. Electron Dev. **36**, 1303–1310.
71) Pourmand, N., Karhanek, M., Persson, H.H.J. and Davis, R.W. (2006) Direct electrical detection of DNA synthesis. Proc. Natl. Acad. Sci. U.S.A. **103**, 6466–6470.
72) Miyahara, Y., Tsukada, K., Miyagi, H. and Simon, W. (1991) Urea sensor based on an ammonium ion-sensitive field effect transistor. Sens. Actuat. B **3**, 287–293.
73) Simon, W. (1971) Ion selective sensors. Pure Appl. Chem. **25**, 811–824.
74) Cuartero, M., Colozza, N., Fernández-Pérez, B.M. and Crespo, G.A. (2020) Why ammonium detection is particularly challenging but insightful with ionophore-based potentiometric sensors – an overview of the progress in the last 20 years. Analyst **145**, 3188–3210.
75) Sakata, T. and Miyahara, Y. (2005) Potentiometric detection of single nucleotide polymorphism by using a genetic field effect transistor. ChemBioChem **6**, 703–710.
76) Sakata, T. and Miyahara, Y. (2007) Direct transduction of allele-specific primer extension into electrical signal using genetic field effect transistor. Biosens. Bioelectron. **22**, 1311–1316.
77) Sakata, T. and Miyahara, Y. (2008) Noninvasive monitoring of transporter-substrate interaction at cell membrane. Anal. Chem. **80**, 1493–1496.
78) Sakata, T. and Miyahara, Y. (2006) DNA sequencing based on intrinsic molecular charges. Angew. Chem. Int. Ed. **45**, 2225–2228.
79) Juang, D.S., Lin, C.H., Huo, Y.-R., Tang, C.-Y., Cheng, C.-R., Wu, H.-S. *et al.* (2018) Proton-ELISA: Electrochemical immunoassay on a dual-gated ISFET array. Biosens. Bioelectron. **117**, 175–182.
80) Schaffhauser, D.F., Patti, M., Goda, T., Miyahara, Y., Forster, I.C. and Dittrich, P.S. (2012) An integrated field-effect microdevice for monitoring membrane transport in xenopus laevis oocytes via

lateral proton diffusion. PLoS One **7**, e39238.
81) Schaffhauser, D.F., Fine, M., Tabata, M., Goda, T. and Miyahara, Y. (2016) Measurement of rapid amiloride-dependent pH changes at the cell surface using a proton-sensitive field-effect transistor. Biosensors **6**, 11.
82) Imaizumi, Y., Goda, T., Toya, Y., Matsumoto, A. and Miyahara, Y. (2016) Oleyl group-functionalized insulating gate transistors for measuring extracellular pH of floating cells. Sci. Technol. Adv. Mater. **17**, 337–345.
83) Imaizumi, Y., Goda, T., Schaffhauser, D.F., Okada, J., Matsumoto, A. and Miyahara, Y. (2017) Proton-sensing transistor systems for detecting ion leakage from plasma membranes under chemical stimuli. Acta Biomater. **50**, 502–509.
84) Horiguchi, Y., Goda, T., Matsumoto, A., Takeuchi, H., Yamaoka, S. and Miyahara, Y. (2017) Direct and label-free influenza virus detection based on multisite binding to sialic acid receptors. Biosens. Bioelectron. **92**, 234–240.
85) Hatano, H., Goda, T., Matsumoto, A. and Miyahara, Y. (2019) Induced proton perturbation for sensitive and selective detection of tight junction breakdown. Anal. Chem. **91**, 3525–3532.
86) Otsuka, H. (2010) Nanofabrication of nonfouling surfaces for micropatterning of cell and microtissue. Molecules **15**, 5525–5546.
87) Tabata, M., Liu, X., Khamhanglit, C., Kotaki, S. and Miyahara, Y. (2022) Detection of epidermal growth factor receptor expression in breast cancer cell lines using an ion-sensitive field-effect transistor in combination with enzymatic chemical signal amplification. J. Am. Chem. Soc. **144**, 16545–16552.
88) Tabata, M., Khamhanglit, C., Kotaki, S. and Miyahara, Y. (2022) Detection of cell membrane proteins using ion sensitive field effect transistors combined with chemical signal amplification. Chem. Commun. **58**, 7368–7371.
89) Otsuka, H., Nagamura, M., Kaneko, A., Kutsuzawa, K., Sakata, T. and Miyahara, Y. (2012) Chondrocyte spheroids on microfabricated PEG hydrogel surface and their noninvasive functional monitoring. Sci. Technol. Adv. Mater. **13**, 064217.
90) Yoshioka, Y., Kosaka, N., Konishi, Y., Ohta, H., Okamoto, H., Sonoda, H. *et al.* (2014) Ultrasensitive liquid biopsy of circulating extracellular vesicles using ExoScreen. Nat. Commun. **5**, 3591.
91) Im, H., Shao, H.L., Park, Y.I., Peterson, V.M., Castro, C.M., Weissleder, R. *et al.* (2014) Label-free detection and molecular profiling of exosomes with a nano-plasmonic sensor. Nat. Biotechnol. **32**, 490–495.
92) Spanu, S., van Roeyen, C.R., Denecke, B., Floege, J. and Mühlfeld, A.S. (2014) Urinary exosomes: a novel means to non-invasively assess changes in renal gene and protein expression. PLoS One **9**, e109631.
93) Miyahara, Y. (1998) Intelligent and micro ion sensors. IEEJ Transactions on Sensors and Micromachines **118**, 548–551.
94) Miyahara, Y., Tsukada, K. and Miyagi, H. (1988) Field-effect transistor using a solid electrolyte as a new oxygen sensor. J. Appl. Phys. **63**, 2431–2434.
95) Miyahara, Y. (1992) Characterization of sputtered yttria-stabilized zirconia thin film and its application to a metal-insulator-semiconductor structure. J. Appl. Phys. **71**, 2309–2314.
96) Han, J.-H., Kim, K.B., Kim, H.C. and Chung, T.D. (2009) Ionic circuits based on polyelectrolyte diodes on a microchip. Angew. Chem. Int. Ed. **48**, 3830–3833.
97) Bolin, M.H., Svennersten, K., Nilsson, D., Sawatdee, A., Jager, E.W.H., Richte-Dahlfors, A. *et al.* (2009) Active control of epithelial cell-density gradients grown along the channel of an organic electrochemical transistor. Adv. Mater. **21**, 4379–4382.
98) Terabe, K., Hasegawa, T., Nakayama, T. and Aono, M. (2005) Quantized conductance atomic switch. Nature **433**, 47–50.
99) Gumyusenge, A. (2022) Organic iono-electronics, a new front for semiconducting polymers to shine. Acc. Mater. Res. **3**, 669–671.
100) Carrad, D.J., Mostert, A.B., Ullah, A.R., Burke, A.M., Joyce, H.J., Tan, H.H. *et al.* (2017) Hybrid nanowire ion-to-electron transducers for integrated bioelectronic circuitry. Nano Lett. **17**, 827–833.

(Received June 28, 2023; accepted Sep. 25, 2023)

Profile

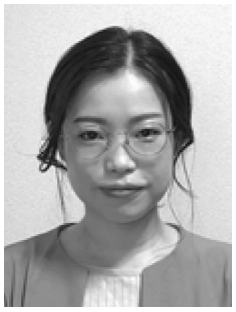

Miyuki Tabata received her PhD from the Graduate School of Pure and Applied Sciences, University of Tsukuba. She then began working at the Tokyo Medical and Dental University in the laboratory of Bioelectronics (Prof. Yuji Miyahara). She has been a PI at the Tokyo University of Agriculture and Technology since 2023. Her research focuses on developing electrical/electrochemical biosensing devices and their medical applications.

Profile

Yuji Miyahara was born in Kanagawa Prefecture in 1956. He graduated from the School of Engineering, Tokyo Institute of Technology in 1980 and received his PhD from Tokyo Institute of Technology in 1985. He joined the Hitachi Central Research Laboratory in 1985. He was a visiting researcher at the Swiss Federal Institute of Technology from 1988 to 1989. He became the group leader of the Bioelectronics group and a director of the Biomaterials Center at the National Institute for Materials Science in 2002 and 2008, respectively. He became a professor at the Institute of Biomaterials and Bioengineering, Tokyo Medical and Dental University in 2010, and a director of the Institute of Biomaterials and Bioengineering, Tokyo Medical and Dental University in 2014. He has been a specially appointed professor at Tokyo Medical and Dental University since 2022. He has been working in the fields of electronics and biotechnology for more than 40 years. He has been studying bio-transistors for DNA analyses, micro total analysis systems (μTAS), and solid-state biosensors. He received the Prize of Progress from The Institute of Electrical Engineers of Japan in 2005, and the Yamazaki Teiichi Prize from the Foundation for Promotion of Material Science and Technology of Japan in 2006.